Aus der Klinik für Herz-, Thorax- und Gefäßchirurgie
des Deutschen Herzzentrums Berlin

DISSERTATION

Quantitative evaluation of the mitral valve anatomy, geometry and spatial relationships in multiple cardiac phases by multi-slice computed tomography for planning of minimally invasive or percutaneous interventions

zur Erlangung des akademischen Grades
Doctor medicinae (Dr. med.)

vorgelegt der Medizinischen Fakultät
Charité – Universitätsmedizin Berlin

von

Leyla Musayeva

aus Baku, Aserbaidschan

Datum der Promotion: 21.06.2020

Contents

List of tables 4
List of figures 5
Abbreviations and Acronyms 6
Abstract in German (Zusammenfassung) 8
Abstract in English (Summary) 10
1 INTRODUCTION 12
1.1 Background 12
1.2 Mitral valve anatomy 12
1.3 Mitral regurgitation 14
1.4 Overview of imaging techniques 15
1.5 MR treatment options 17
2 STUDY OBJECTIVES 20
3 MATERIALS AND METHODS 21
3.1. Study population 21
3.2. CT protocol for data acquisition 21
3.3. Data reconstruction 22
3.4. Data analysis 22
3.5. Statistical analysis 33
4. RESULTS 33
4.1 Baseline characteristics 33
4.2 Systolic and diastolic LV sphericity index 34
4.3 Mitral annulus dimensions 35
4.4 Aorto-mitral angle 48
4.5 Annulus to papillary muscles distances 48
4.4. LA-to-LV axis angle 49
4.5 Mitral annular dynamics (mobility of the MA) 50
5. DISCUSSION 52
5.1 Interpretation of the study results and their significance 52
5.2. Comparison of results with earlier studies 53
5.3 The advantages of CTA in evaluating the MV and comparison with other clinical imaging procedures 56
5.4 Study limitations 57
6. Conclusion 58
Bibliography (references) 59
Affidavit 68

Curriculum Vitae 69
Acknowledgements 71

List of tables

Table 1: Baseline characteristics and volumetric parameters of the study population

Table 2: Annulus surface (As) values in the S-shaped mitral annulus model for both groups

Table 3: Entire circumference (3D-Ps) in the S-shaped mitral annulus model for both groups

Table 4: Projected circumference of the entire saddle-shaped annulus (2D-Ps) for both groups in all phases of the cardiac cycle

Table 5: Summary of the projected distance from the aortic peak to the posterior peak (SLs)

Table 6: Summary of entire anterior circumference (3D-Ps anterior) of the MA for both groups

Table 7: Summary of the entire posterior circumference (3D-Ps posterior) of the MA for both groups

Table 8: Summary of the projected anterior circumference (2D-Ps anterior) of the MA

Table 9: Projected posterior circumference (2D-Ps posterior) for both groups

Table 10: Summary of MA surface dimensions in the D-shaped MA model (Ad) for every 10% phase of the cardiac cycle

Table 11: Projected distance from the aortic peak to the posterior peak in the D-shaped mitral annulus model (SLd)

Table 12: Trigone-to-trigone (TT) distance representing the anterior border of the MA in the D-shaped model

Table 13: Mean values of the mitral annulus mobility

List of figures

Figure 1: Assessment of LV endocardial and epicardial borders

Figure 2: Exemplary table with LV volumetric parameters

Figure 3: Measurement of LV long-axis length in 2-chamber view, reformatted images

Figure 4: Tracing of LA cavity area in end-systolic 2-chamber and 4-chamber MPR views

Figure 5: Saddle-shaped MV annulus defined using 3mensio imaging software

Figure 6: Saddle-shaped MV annular 3D segmentation and parameters in systole

Figure 7: Saddle-shaped mitral annulus height measurement using 3mensio imaging software

Figure 8: Representative example of a D-shaped mitral annulus assessment

Figure 9: Aortic root 3 nadirs defined using 3mensio imaging software

Figure 10: Measurement of the aorto-mitral angle

Figure 11: 3-chamber view MPR with angle tool for measuring LA-to-LV axis

Figure 12: LV sphericity index in diastole and in systole for both groups

Figure 13: Difference in mitral annulus entire circumference for the saddle-shaped annulus (3D-Ps)

Figure 14: Difference in the mitral annulus height for the saddle-shaped annulus (Hs) and fluctuations thereof during the cardiac cycle

Figure 15: Summary of dimensions of the mitral annulus entire circumference of the D-shaped annulus (3D-Pd) for every 10% phase of the cardiac cycle

Figure 16: Projected circumference of the D-shaped annulus

Figure 17: Mean values of MA dimensions for saddle-shaped and D- shaped approaches in systole and diastole

Figure 18: Mean values of the aorto-mitral angle for both groups

Figure 19: LA-to-LV axis angle mean values for both groups

Figure 20: MA mobility: Anteroposterior-distances (SLs-distance 3D) for both groups in all cardiac cycle phases

Figure 21: MA mobility: 3D entire circumference values for the saddle-shaped annulus for both groups in all cardiac cycle phases

Abbreviations and Acronyms

2D-Pd	projected circumference of the entire D-shaped annulus
2D-Ps	projected circumference of the entire saddle-shaped annulus
3D	3-dimensional
3D-Pd	entire circumference of the D-shaped annulus
3D-Ps	entire circumference of the saddle-shaped annulus
Ad	mitral valve D-shaped annulus area
AMA	aorto-mitral angle
AML	anterior mitral leaflet
As	projected annulus area of the saddle-shaped mitral annulus
BMI	body mass index
CABG	coronary artery bypass graft
CAD	coronary artery disease
CI	cardiac index
CMR	cardiac magnetic resonance
CO	cardiac output
CPB	cardiopulmonary bypass
CRT	cardiac resynchronization therapy
CT	computed tomography
CTA	computed tomography angiography
DMR	degenerative mitral regurgitation
FMR	functional mitral regurgitation
EF	ejection fraction
HF	heart failure
Hs	saddle-shaped annular height
LA	left atrium / left atrial
LV	left ventricle / left ventricular
LVEDD	end-diastolic diameter
LVEDV	left ventricular end-diastolic volume
LVEDVI	left ventricular end-diastolic volume index
LVESVI	left ventricular end-systolic volume index
LVEF	left ventricular ejection fraction

LVESV	left ventricular end-systolic volume
LVOT	left ventricular outflow tract
MA	mitral valve annulus
MPR	multiplanar reconstruction
MR	mitral regurgitation
MSCT	multi-slice computed tomography
MV	mitral valve
NYHA	New York Heart Association
OMT	optimal medical therapy
PM	papillary muscle
PML	posterior mitral leaflet
SL	septal-to-lateral
SLd	septal-to-lateral distance of D-shaped annulus
SLs	septal-to-lateral distance of saddle-shaped annulus
SV	stroke volume
TAVI	transcatheter aortic valve implantation
TEE	transesophageal echocardiography
TMVI	transcatheter mitral valve implantation
TMVR	transcatheter mitral valve replacement
TT	trigone-to-trigone
TTE	transthoracic echocardiography

Abstract in German (Zusammenfassung)

Ziel: Ziel dieser Studie war die Beurteilung der Mitralklappenanatomie, -geometrie und -beweglichkeit von gesunden Probanden (Kontrollgruppe) und von Patienten mit funktioneller Mitralklappeninsuffizienz (FMR) durch MSCT über den gesamten Herzzyklus mit Fokus auf der Planung von Transkatheter-Mitralklappe Verfahren bei deren Planung das MSCT einen hohen Stellenwert hat.

Material und Methoden: Datensätze von 24 Patienten ohne Mitralklappenerkrankung und 22 Patienten mit FMR, bei denen eine EKG-getriggerte MSCT durchgeführt wurde, wurden retrospektiv ausgewertet. Das Durchschnittsalter betrug 47 ± 11 gegenüber 63 ± 7 Jahren (p <0,05), männliches Geschlecht 75% gegenüber 68% (ns), BMI 26 ± 2,8 kg / m² gegenüber 26 ± 3,5 kg / m² (ns), LVEF 72 ± 6% vs. 31 ± 9% (p <0,05), LVEDD 55,3 ± 5,4 vs. 81 ± 11 mm (p <0,05). Die Ausmessung der Oberfläche des Mitralanulus (MA), des gesamten Umfangs, des projizierten Umfangs des Annulus, der Trigon-Trigon-Distanz und der Septum-zu-Lateralwand-Abstände für den sattelförmigen und D-förmigen Mitralanulus und die Anulushöhe für den sattelförmigen Anulus, den Aorto-Mitralen- Winkel, der Linker Vorhof (LA)-zu- Linker Ventrikel (LV)-Achsenwinkel und der Abstand zwischen MA und Papillarmuskeln wurde für alle Patienten in beiden Gruppen für zehn 10% Phasen Intervallen während des gesamten Herzzyklus durchgeführt.

Ergebnisse: Die mittlere 3D MA-Fläche betrug 12 ± 2 cm² in der Kontrollgruppe und 14,6 ± 0,52 cm² bei Patienten mit FMR, die D-förmige Anulusfläche war 10,3 ± 1,6 cm² und 12,7 ± 0,5 cm². Diese Werte waren zwischen den zwei Gruppen und beiden Methoden signifikant unterschiedlich. Der Trigon-zu-Trigon-Abstand war bei Patienten mit FMR signifikant größer als bei gesunden Probanden; 33,7 ± 1,9 mm vs. 34,6 ± 4 mm (P <0,05). Der mittlere Aorten–Mitralwinkel lag bei gesunden Probanden bei 55 ± 7° gegenüber 46 ± 6,8° bei Patienten mit FMR. Darüber hinaus ist die Beweglichkeit des Mitralanulus bei gesunden Probanden höher als bei Patienten mit FMR.

Schlussfolgerung: Es gibt signifikante Unterschiede in der Mitralanulus-Morphologie zwischen gesunden Probanden und Patienten mit FMR sowie der Morphologie bzw. Beweglichkeit des Mitralanulus während des gesamten Herzzyklus. Anbetracht der geringen Beweglichkeit des Mitralanulus bei Patienten mit FMR und seiner größten Größe in der diastolischen Phase könnte die mehrphasige MSCT bei der Planung einer TMVI beispielsweise durch zweiphasige Scans ersetzt werden. Dies spielt eine wichtige Rolle bei der präprozeduralen Analyse und bei der Reduzierung der Strahlendosis, jedoch ist die Verwendung von Mehrphasen-CTA in

komplizierten Fällen sicher immer von Vorteil. Zusammenfassend zeigt unsere Studie, dass eine nicht-invasive und umfassende Beurteilung der Mitralklappe mittels MSCT möglich ist.

Schlüsselwörter: Mitralklappe, Mitralanulus, Mobilität, funktionelle Mitralinsuffizienz, Computertomographie, Transkatheter-Mitralklappenersatz.

Abstract in English (Summary)

Objective: The objective of this study was to assess the mitral valve anatomy, geometry and mobility of control group and of patients with functional mitral regurgitation (FMR) by MSCT throughout the entire cardiac cycle in regards of optimizing the planning of transcatheter mitral valve procedures.

Materials and methods: 24 healthy patients vs. 22 patients with varying degrees of FMR who had undergone ECG gated CTA were evaluated retrospectively. The mean age was 47 ± 11 vs. 63 ± 7 years ($p<0.05$), male gender 75% vs. 68% (ns), BMI 26 ± 2.8 kg/m² versus 26 ± 3.5 kg/m² (ns), LVEF 72 ± 6% vs. 31 ± 9% ($p<0.05$), LVEDD 55.3 ± 5.4 vs. 81 ± 11 mm ($p<0.05$). The evaluation of MA surface, entire circumference, projected circumference, trigone-to-trigone distance, and septal-to lateral distances for saddle-shaped and D-shaped mitral annulus, and annulus height for saddle-shaped annulus, aorto-mitral annular angle, LA to LV axis angle and MA to papillary muscles distance was carried out for all patients in both groups for ten 10% intervals throughout the cardiac cycle.

Results: The mean MA saddle-shaped annular area averaged 12 ± 2 cm² in the control group, 14.6 ± 0.52 cm² in patients with FMR, the D-shaped annular area averaged 10.3 ± 1.6 cm² vs. 12.7 ± 0.5 cm², respectively, thus representing a significant difference between the two groups and both models. The trigone-to-trigone distance was slightly larger in patients with FMR than in healthy subjects, namely 33.7 ± 1.9 mm vs. 34.6 ± 0.4 mm ($p<0.05$). The aorto-mitral angle mean for healthy subjects was 55 ± 7° vs. 46 ± 6.8° in patients with FMR. The mobility of the mitral annulus was higher in healthy patients than in patients with FMR.

Conclusion: This study showed that there are significant differences in the mitral annular morphology between controls and patients with FMR, as well as several changes between different sizing approaches of the mitral annulus throughout the entire cardiac cycle.
Considering the low mobility of the mitral annulus in patients with FMR and its biggest size in diastolic phase, multiphase MSCT might be replaced by dual-phase scans for example when planning TMVI. This plays an important role in timing the pre-procedural analysis and in reducing radiation dose. However, using multiphase CTA should still be the favored mode in complicated cases. In summary, our study demonstrates that a non-invasive and comprehensive assessment of the mitral valve by MSCT is feasible.

Key Words: mitral valve, mitral annulus, mobility, functional mitral regurgitation, computed tomography, transcatheter mitral valve replacement.

1 INTRODUCTION

1.1 Background

Mitral valve disease is one of the most prevalent valvular heart diseases causing significant mortality and morbidity. The mitral valve is the left-sided bicuspid atrioventricular valve. It consists of anterior and posterior leaflets and separates the left atrium from the left ventricle. Embryologically, it forms from the endocardial cushions between the 5th and 8th week of development (1). Symmetrical apposition (a minimal overlap of about 4-5 mm) and complete coaptation of both leaflets is essential in preventing regurgitation (2). Mitral regurgitation (MR) affects almost every 1 in 10 individuals over 75 years of age (3-5).

1.2 Mitral valve anatomy

The MV apparatus is a dynamic and complex anatomical structure (6). It consists of the three-dimensional, non-circular, saddle-shaped, highly dynamic mitral annulus, anterior and posterior mitral valve leaflets, a highly individualized subvalvular apparatus (fibrous tendinous chords and the papillary muscles), the left ventricle (LV) and the left atrium (LA). Any abnormality in any of these components may cause mitral dysfunction (7). The MV is very closed to the left ventricular outflow tract (LVOT), the left circumflex artery and the coronary sinus (8). Thus, a detailed pre-procedural analysis is imperative for patient selection and preoperative procedural planning.

1.2.1 Mitral annulus and leaflets

The mitral annulus is a complex and nonplanar geometric structure with a greater commissural diameter (long axis) and a smaller septolateral diameter (short axis) (1). The normal mitral annulus is non-planar and saddle-shaped fibrous ring (9). Both leaflets are attached to the annulus ring. The anterior leaflet is anchored to the fibrous part of the annulus. The anterior part of the annulus by its fibrous nature is more rigid than the posterior part and is very closely associated with the aortic annulus (10). The posterior part is muscular and thus prone to pathological ventricular remodeling (2). The anterior mitral leaflet has a triangular shape and is usually larger and thicker than the posterior one. The aortic fibrous continuity of the anterior mitral leaflet is known as the aortic mitral curtain. The posterior leaflet has a longer attachment to the annulus (2). Using the Carpentier nomenclature, the indentations of the free edge of the posterior leaflet are defining three scallops; P1 is the most lateral scallop, P2 the middle scallop, and P3 the most medial scallop (11). The anterior leaflet has no indentation and is divided into the three zones located opposite the posterior scallops (known as A1, A2 and A3, respectively)

(12-14). The points where leaflets are attached to each other are known as posteromedial and anterolateral commissures. Fibrous thickening external to the mitral valve commissures are called trigones.

1.2.2 Subvalvular apparatus

The mitral leaflets are connected to papillary muscles by the chordae tendineae (14). The anatomy of the subvalvular apparatus is highly variable because of multiple anatomic variations in the posterior papillary muscle (PM) and the number of chordae tendineae. The anterior PM has a single insertion, whereas the posterior PM exhibits multiple heads and insertions (7). There are three main groups of morphological variants of the papillary muscle anatomy (15). In the first group, PM has one head and one insertion part (10, 15). PMs with apical part divided into two heads along a sagittal plane belong to the second group. The ventral head is related to the anterior leaflet of the mitral valve and the dorsal head gives rise to the chordae tendineae supporting the posterior leaflet. The conjoined parts of the two heads are connected to the commissural zone (10). PMs with three or more heads make up the third group (7). The head related to the commissural zone is found between the ventral and dorsal heads. The dorsal head supports the posterior leaflet and the ventral head supports the anterior leaflet of the mitral valve (10). The second and third groups also have several subtypes, demonstrating just how variable the anatomy of the PM is (7, 15, 16). The superolateral papillary muscle is supplied by one or more branches of the circumflex artery, or by diagonal branches, whereas the inferoseptal papillary muscle is supplied by a single branch of the circumflex or right coronary artery, depending on the coronary artery dominance. Because of its single vascular supply, the inferoseptal muscle is susceptible to coronary ischemia (5, 17).

The fibrocollagenous tendinous cords, or chordae tendineae, originate from the papillary muscles, bifurcate several times, and attach to the free edges and ventricular aspects of both leaflets, thus preventing marginal prolapse and aligning the zone of coaptation (18). The posteromedial PM chords attach to the medial half of both MV leaflets (i.e. posteromedial commissure, P3, A3 and half of P2 and A2). Similarly, the anterolateral PM gives chords to the lateral half of the leaflets (i.e. anterolateral commissure, A1, P1 and half of P2 and A2) (2). The chords are thinnest at their sites of insertion in the leaflets, and this is the site of predilection for chordal rupture. There are three types of chordae tendineae depending on their attachment (2, 18). Primary chords attach to the free edge of the rough zone of the leaflets. They maintain the leaflet apposition and valve closure and their dysfunction leads to an acute MR (19). Secondary chords attach to the ventricular surface of the leaflet in the region of the rough zone (18). The

largest and thickest two of the secondary chords of the anterior mitral leaflet called strut chords and arise from the tip of each papillary muscle and are thought to be the strongest (2, 18). They are responsible for the fibrous continuity of the mitral annulus with the left ventricular myocardium. Strut chords are under constant tension and maintaining the shape and size of the left ventricle. Their transection results in alterations in the left ventricular geometry and can lead to left ventricular remodeling (17). The tertiary chords (the basal chords) are found in the mural (posterior) leaflet only which has a basal zone, and attach directly to the ventricular wall (17, 20).

1.3 Mitral regurgitation

A reduction or elimination of the normal systolic coaptation between anterior and posterior mitral leaflets are the cause of mitral regurgitation in all cases, and a particular cause might produce regurgitation by different mechanisms (21). MR can generally be classified as ischemic and non-ischemic based on the underlying pathology, or based on the mechanism, which is generally divided into two types: primary (organic) MR and secondary (functional) MR.

The classification proposed by Carpentier in 1972 described three classic mechanisms of MR (11). According to classification, MR without pathologic leaflet motion should be described as Type I dysfunction. It occurs due to pathologies such as annular dilatation or leaflet perforation (11, 20, 22). MR due to excessive leaflet motion from degenerative changes of the leaflets or chordae tendineae should be described as Type II dysfunction (11, 23). Type III dysfunction occurs due to restricted leaflet motion (leaflet tethering) caused by rheumatic disease or displacement of papillary muscles secondary to left ventricular dilatation (23, 24).

Non-ischemic primary mitral regurgitation is called degenerative mitral regurgitation (DMR) (Carpentier type II dysfunction) and is caused by a primary abnormality of components of the mitral valve apparatus, such as chordae tendineae rupture (fibroelastic deficiency, traumatic, or due to endocarditis), congenital leaflet cleft, inflammatory changes, myxomatous leaflet disease, iatrogenic injury due to radiation or drugs, or calcification of the mitral annulus (24). Myxomatous degeneration is seen more frequently in younger patients, is usually associated with mitral annulus dilatation and characterized by a redundancy of tissue that appears to be myxomatous in histopathological analysis (25). Fibroelastic degeneration is generally seen in elderly patients and is characterized by a single lesion without tissue redundancy. In such patients, the mitral annulus is found to be normal or slightly dilated (26).

Secondary or functional MR (FMR) is seen in mitral leaflets that are structurally intact but show tethering and retraction of the leaflet bodies (27) due to changes in the ventricular geometry

resulting in failure of leaflet coaptation due to other cardiac diseases, such as ischemic or dilated cardiomyopathy, myocarditis or any other cause of LV dysfunction. Recent investigations, however, show significant MV leaflet tissue changes (extracellular matrix changes) and an increased leaflet thickness and length as signs of structural leaflet remodeling (28, 29). Several underlying mechanisms may contribute to FMR. These include LV remodeling, wall motion abnormalities, displacement of the papillary muscles, or deformation of the mitral annulus (7, 21, 30).

Based on clinical findings, MR can be acute or chronic (27). Ischemic MR is frequently chronic and functional. Acute ischemic MR may present due to papillary muscle infarction and rupture. In acute MR, there is no progressive adaptation of the left atrium to the sudden volume overload. This leads to a rapid increase of the left atrial and pulmonary venous pressure and results in acute pulmonary edema (21).

The chronic form of ischemic MR usually occurs more than one week after myocardial infarction with LV wall motion abnormalities. In chronic MR, the left atrium adapts to the persistent volume overload. Due to prolonged volume overload, the left ventricle may over time dilate and lose contractile efficiency, which may lead to MV annulus dilatation and result in chronic heart failure (21). Patients with primary MR due to a leaflet pathology (myxomatous, rheumatic, or other) have a better long-term prognosis and should not be included in the group of patients with chronic IMR (27).

1.4 Overview of imaging techniques

The progress in cardiac imaging led to improvements in the scientific assessment of the anatomy, physiology, and pathophysiology of the MV. The valuable and defining role of 3D echocardiography, multi-slice computed tomography (MSCT) and cardiac magnetic resonance (CMR) imaging in evaluating the MV and the development and performance of transcatheter valvular therapies has been demonstrated (31).

Echocardiography is the current gold standard for assessing the cardiac valves and is used as a first-line imaging technique to study mitral valve disease (32). The mitral valve can be evaluated by transesophageal echocardiography (TEE) or by transthoracic echocardiography (TTE). It is cost-effective, widely accessible, offers excellent temporal resolution and in most cases delivers adequate information for therapy planning, particularly by providing a so-called “surgical view” (33). Echocardiography has several limitations, including operator dependence and poor acoustic window in some patients, and interference with catheters during percutaneous procedures like the Mitraclip intervention. Moreover, some studies have shown underestimation of the

volumetric parameters and overestimation of the LV ejection fraction as assessed by echocardiography (34). Additionally, for TEE, orotracheal intubation and general anesthesia is sometimes necessary (17).

More recently, techniques such as multi-slice computed tomography (MSCT) and cardiac magnetic resonance (CMR) imaging are also widely used to study the mitral valve. These techniques can answer dedicated questions about paravalvular changes, associated aortic and myocardial diseases.

Magnetic resonance imaging is a non-invasive imaging modality that does not expose the patient to ionizing radiation (32, 35). It is now established as the gold standard for a comprehensive assessment of the myocardium. It is also the reference standard for detailed non-invasive measurements of the left and right ventricular function and blood flow quantification (34). The main indication for CMR is myocarditis and cardiomyopathy, the second main indication is exclusion of coronary artery disease with stress tests. Advanced techniques such as T1 mapping and tagging of MR are widely used nowadays and significantly improve the sensitivity of CMR in myocardial assessments (36-38). In valves affected by stenosis or regurgitation, CMR allows both qualitative and quantitative assessments (35). However, there are several contraindications for using CMR imaging in certain patients (e.g., those with implanted devices such as a pacemaker, claustrophobia and arrhythmias that can affect ECG gating) (35).

In recent years, computed tomographic angiography (CTA) has made impressive progress in cardiac imaging. By its widespread availability, high reproducibility and relative operator-independence, CTA becomes useful tool in cardiac imaging (39).CTA enables volume rendering and other reconstruction techniques which enable a detailed visualization of the cardiovascular anatomy in congenital heart diseases as well as anatomical and dynamic changes in the heart valves. It can be used as an alternative to MRI for quantification of the LV and RV function in patients with contraindications for MRI or patients who are not capable of holding their breath for longer periods (34). The spatial resolution of CT is excellent and is superior to the resolution of magnetic resonance imaging (MRI) (40). The main established clinical application of MSCT in cardiac imaging is the evaluation of the coronary arteries and aorta. The use of ECG-gated CT angiographies allows a simultaneous assessment of the cardiac anatomy and pathology, valvular morphology, coronary arteries, major arteries and, moreover, the mediastinum and the area surrounding the lungs (7, 41).

Fast imaging time and high spatial resolution of CTA, allowing for high quality 2D and 3D reconstructions of the mitral valve and subvalvular apparatus at any time point of the cardiac cycle (42). The short acquisition time (10-15 seconds) makes MSCT a useful tool for planning

surgical and interventional procedures for patients suffering from high-grade dyspnea (6, 43, 44).

The one of the main challenges in cardiac CT is temporal resolution. It is inferior to the temporal resolution of MRI and echocardiography. Improvement in spatial resolution is possible by using of second and third generation dual source MDCT technology. A modern dual-source scanner gives twice as good temporal resolution because data reconstruction is possible with only 90 tube rotation and can yield a temporal resolution less than 80 ms (45). The need for high temporal resolution in cardiac CT requires a low pitch, which increases radiation dose. The use of ionizing radiation is another limitation of CTA in valve assessment. Retrospective ECG-gated CT angiography is essential for obtaining cine images despite its association with a higher radiation exposure. Nowadays, techniques such as ECG-triggered CTA with radiation dose modulation are widely used and offer optimal visualization of the desired cardiac phase with a reduced dose in other parts of the cardiac cycle (35). Visualization of thin leaflets and chordae tendineae is limited by CTA (17). Moreover, CTA does not provide a direct measure of the valvular pressure gradient, which could be considered another limitation (35).

1.5 MR treatment options

The choice of the best treatment for patients with MR is very important. The purpose of medical and/or surgical therapy are to amend heart failure symptoms and to improve both LV remodeling and function, as well as the outcome (46). Standard conservative treatment options are optimal medical therapy (OMT) and cardiac resynchronization therapy (CRT) (47, 48). Pharmacotherapy (e.g. diuretics, vasodilators, etc.) aims to prevent organic diseases (49). CRT is the recent advancement in heart failure (HF) treatment. As shown by multiple randomized trials, there are outstanding clinical benefits associated with the use of CRT as a treatment method for selected patients with chronic HF (48, 50, 51). Surgical repair or replacement are the pillars of therapy for mitral regurgitation (MR) whenever conservative strategies fail to improve the symptoms and the severity increases (52). According to Kang et al. early surgery is associated with a significant long-term reduction of cardiac mortality and cardiac events in asymptomatic patients with severe MR, compared to conservative management (53). Minimally invasive surgical procedures (e.g. right minithoracotomy approaches, etc.) were developed to decrease patients' morbidity and postoperative complications (54, 55).

DMR is the most common form of MR referred for surgical correction. Surgical intervention for degenerative MR includes multiple techniques, such as leaflet repair with resection, chordal transfer, use of polytetrafluoroethylene neochordae, prosthetic ring or band annuloplasty and

mid-late systolic clicks (56). Patients with FMR universally have left ventricular dysfunction; they frequently suffer from concomitant heart failure and have a poorer prognosis than those with DMR. Unlike for DMR, surgical correction has not become the standard of care of FMR. Patients with FMR generally have an increased higher surgical risk, and although surgical correction of FMR has been shown to improve the functional class and left ventricular remodeling, a survival benefit has not been demonstrated (57, 58).

Several recent papers show poor mid- and long-term results of surgical MV repair and replacement in patients with FMR and a severely reduced left ventricular ejection fraction (23, 59-61). The results reported by Acker et al. (59) showed no significant differences in mortality at 30 days or 12 months between mitral repair and mitral replacement groups. The observed 30-day death rates reported by the Acker group (1.6% in the repair group and 4.0% in the replacement group) were lower than the national rates reported by the Society of Thoracic Surgeons (5.3% and 8.5% for repair and replacement with CABG, respectively) (59). Restrictive annuloplasty is the most commonly adopted surgical procedure that improves heart failure symptoms in patients with chronic ischemic MR (46). A major limitation of current surgical annuloplasty techniques is that moderate or severe MR recurs in up to one-third of treated patients within one year of surgery (23, 62). Long aortic cross-clamping and cardiopulmonary bypass (CPB) have an independent impact on mortality risk. This has to be kept in mind when selecting the appropriate procedure based on the patient's status (63).

The number of patients with ischemic heart disease or cardiomyopathies which lead to FMR increases with advancing age, such that FMR is more frequent than organic MV disorders (47).

Chronic functional/ischemic mitral regurgitation is associated with poor long-term survival (27). Hence, in patients with an unacceptably high surgical risk (e.g. those with significant comorbidities), innovative transcatheter concepts (minimally invasive procedures) may be a viable option.

Minimally invasive methods for treating MR currently include transcatheter leaflet repair (MitraClip [Abbott Vascular, Santa Clara, CA], Mobius [Edwards Life Sciences, Irving, California] etc.), chordal implantation using the NeoChord device (NeoChord, Inc, Eden Prairie, MN), annular shape changes approaches (indirect and direct percutaneous annuloplasty techniques), left ventricular reshaping using iCoapsys (Myocor, Maple Grove, MN, USA) or BACE devices (Mardil, Inc., Morrisville, North Carolina), and transcatheter mitral valve replacement. Among the current percutaneous treatment options, edge-to-edge MV repair, e.g. using the MitraClip procedure, is widely adopted (64-66). The MitraClip is a relatively safe procedure that can be performed even in high surgical risk patients (23). As Answer et al.

reported, percutaneous MitraClip repair is effective but associated with a higher risk of residual MR, and should only be considered in selected patients after careful deliberation (64). The optimal morphological and anatomical criteria for the MitraClip are a centrally located jet (A2-P2 scallop), absence of valve calcification and the size of the mitral valve area (>4 cm^2), etc. (67, 68).

In patients with mitral valve areas <4.0 cm^2 and extensive annular and leaflet calcification, the MitraClip may still be considered as a therapeutic procedure if the clinical benefits outweigh the risks (23).

Transcatheter mitral valve implantation (TMVI) is another minimally invasive procedure that does not require CPB or an aortic X clamp; however, this procedure is still in its early infancy. According to the 2017 ESC Guidelines, transcatheter MV repair may be considered for symptomatic patients with severe chronic primary MR who are at high surgical risk or are inoperable, and should be discussed by the Heart Team to avoid futile treatment (69).

1.5.1 Transcatheter mitral valve implantation (TMVI)

In recent years, transcatheter mitral valve implantation (TMVI) has evolved as a new therapeutic concept (70, 71). On the one hand, it is a brand-new method and, until now, no devices have been approved yet for the clinical application. On the other hand, this technique holds great potential as an alternative therapy for high-risk patients (71). The 2017 update of the 2014 joint guideline of the American College of Cardiology and American Heart Association (ACC/AHA) stated that transcatheter MV repair may be considered for severely symptomatic patients (NYHA class III or IV) with chronic severe primary MR (stage D) who present with a favorable anatomy for the repair procedure and a reasonable life expectancy but have a prohibitive surgical risk due to severe comorbidities and remain severely symptomatic despite optimal management and therapy of HF (72).

Similarly to transcatheter aortic valve implantation (TAVI), patient selection is determined by anatomical and clinical criteria (70). To ensure an appropriate patient selection, it is crucial to have precise parameters of the MV annulus, subvalvular apparatus and LV volumetric data (17, 33, 73).

TMVI systems must be flexible in order to deal with the complex and variable anatomy, provide large effective orifice areas, and be able to handle high transvalvular gradients (17). There are different transcatheter mitral valve implantation systems that have been implanted in humans: CardiAQ valve system (CArdiAQ Valve Technologies, INC.); Tiara valve (Neovasc Inc., Richmond, Canada); FORTIS valve (Edwards Lifesciences, Irvine, CA, USA); Tendyne valve

(Tendyne Inc., Roseville, MN, USA); and Twelve valve (Twelve Inc., Redwood City, CA, USA). All of these implants have a transapical delivery (CardiAQ also transseptal) (70). The Sino Medical AccuFit TMVI system (Sino Medical Sciences Technology, INC.) also offers a transapical delivery and shows a successful device delivery in animal studies; however, it is currently available only in one size (74). The Medtronic transcatheter mitral valve implantation system was studied in animals. This device is delivered via the transatrial approach using a right lateral minithoracotomy. The atrial approach is intended to avoid trauma to the left ventricle, which is a possible risk associated with the transapical approach. The transseptal system is currently in development (75).

Each of the systems mentioned above offers new design solutions to overcome the complex anatomy of the MV apparatus. Considering the complexity of the structure and function of the mitral valve in comparison with the aortic valve, transcatheter mitral therapies still face many barriers. To date, there are many ongoing studies on TMVI systems (70, 74-79). Sophisticated imaging will play a decisive role in transcatheter mitral valve procedures.

It remains unclear which parameters will be relevant for the planning of these procedures. Another challenge in TMVI is the more complex morphology and movement of the mitral valve, especially the mitral annulus, compared to the aortic valve and aortic root. Therefore, the experience gained in transcatheter therapies of the aortic valve cannot be transferred one-to-one to the mitral space.

2 STUDY OBJECTIVES

The goals of this study are a comprehensive assessment of the geometric and anatomical changes of the MV and subvalvular apparatus, the spatial relationships and mobility of the MV in multiple cardiac phases by MSCT in healthy subjects and in patients with FMR, identifying basic differences between groups and sizing strategies in regards of optimizing the planning of transcatheter mitral valve procedures.

3 MATERIALS AND METHODS

3.1. Study population

A total of 46 patients referred to the German Heart Center Berlin for a CTA were retrospectively studied. The study population was divided into two groups; the first group consisted of healthy subjects and the second group of patients with FMR. First group (control group) consists of patients with no known cardiac abnormality, no history of any cardiac disease, cardiac surgery or intervention. They had some CAD risk factors such as dyslipidaemia, hypertension, smoking or positive family history. In these patients it was not possible to exclude CAD by clinical assessment alone and they were referred to coronary CTA. CAD was excluded in all patients in control group. Normal coronary arteries, normal LV volumetric parameters and no LV wall motion abnormalities were reported on their CT exams. Therefore, we believe that the current study population can be, to some extent, a representative sample of normal controls.

In the second group we included patients with FMR because they are much more frequent candidates for minimally invasive procedures. The cardiac CT was performed successfully for both groups between 05 January 2007 and 22 January 2016. All collected data were retrospectively analyzed.

This research was approved by the local ethics committee (number EA4/095/18) and was carried out in accordance with institutional guidelines.

3.2. CT protocol for data acquisition

All patients underwent contrast-enhanced ECG-synchronized cardiac scanning using first- or second-generation dual-source (2x128-slice) scanners (Somatom Definition, Somatom Definition Flash, Siemens AG, Erlangen, Germany) with retrospective ECG triggering to obtain images in all phases of the cardiac cycle (10% phases of the RR interval). CTA was successfully performed in all patients without any reported side effects. Prior to the CT data acquisition, beta-blockers were administered orally or intravenously to some patients to lower the heart rate to 65-70 bpm. This helped improve the image quality by reducing the number of artifacts related to cardiac motion. The study protocol was as follows: tube voltage 100-120 kV, tube current 320 ref. mAs/rotation, rotation time 280 ms (automatic modulation), slice collimation of 128 x 0.6 mm, temporal resolution 75 ms (not depending on the heart rate), slice width 0.75 mm, reconstruction increment 0.4 mm, reconstruction kernel B30f. A total of 80 to 100 ml of non-ionic contrast medium (Imeron 400 mg/ml, Bracco, Altana Pharma, Konstanz, Germany) was generally administered via the antecubital / jugular vein at 4-5 ml/s, followed by saline flush (40

to 50 ml saline at 4-5 ml/s). Automated peak enhancement detection (bolus tracking technique) in the left atrium was used to time the contrast bolus with a start of the data acquisition at a threshold of 160 Hounsfield units. Scans were performed during an inspiration breath hold of 8 to 10 s. The electrocardiogram was recorded simultaneously to allow retrospective ECG synchronization to the cardiac cycle gating and reconstruction of the data at desired phases of the cardiac cycle.

3.3. Data reconstruction

The dataset was reconstructed with a slice thickness of 0.75 mm and a reconstruction increment of 0.4 mm, starting in early systole (0% of the cardiac cycle) all the way to the end-diastole (90% of the cardiac cycle) in steps of 10% of the RR interval.

All datasets were anonymized and transferred to a post-processing workstation for off-line data analysis (syngo.via, Siemens AG).

3.4. Data analysis

Post-processing of the all CT data was analyzed in various cardiac orientations in static and cine images. The LV volumetric analysis was carried out using dedicated CT evaluation software (syngo.via Circulation, Siemens AG) and applying a 3D threshold segmentation algorithm. The end-diastole and end-systole were estimated automatically and adjusted manually if needed. Endocardial borders were traced semi-automatically and papillary muscles were regarded as part of the LV cavity (Figure 1).

Figure 1. Assessment of LV endocardial and epicardial borders in four-chamber view (A), short-axis view (B) and two-chamber view (C), reformatted images.

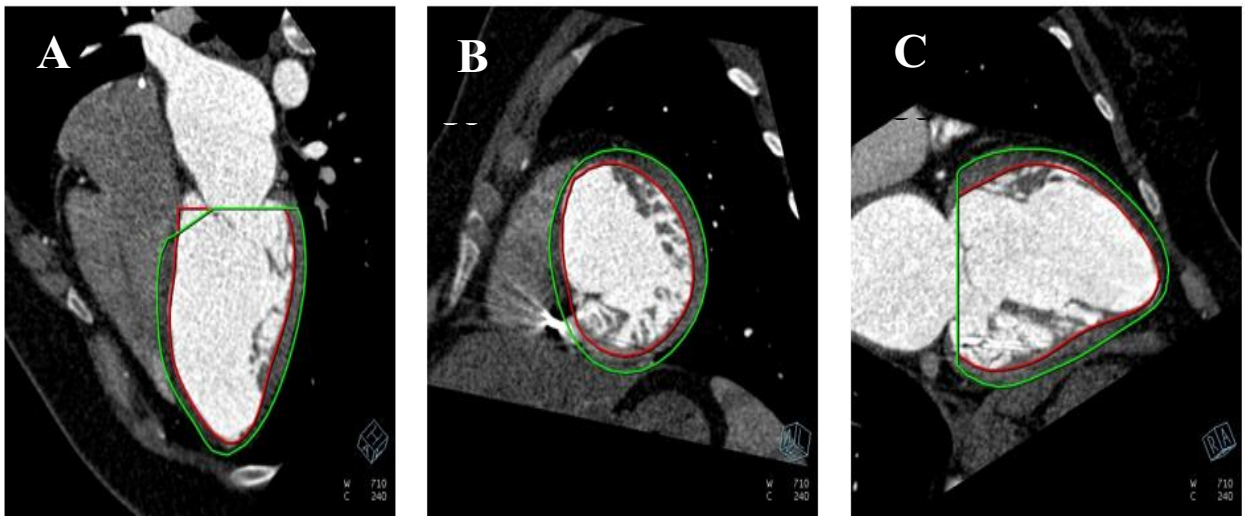

The LV end-diastolic volume (LVEDV) and end-systolic volume (LVESV) were obtained; the left ventricular ejection fraction (LVEF) was calculated by the difference between LVESV and LVEDV divided by LVEDV (Figure 2).

Figure 2. Exemplary table with LV volumetric parameters (A), indexed to BSA volumetric LV parameters (B), the graph of the cardiac cycle (C) and the AHA-conform 17-segment polar maps for visualization of LV wall motion assessed using the syngo.via software (Siemens, Germany).

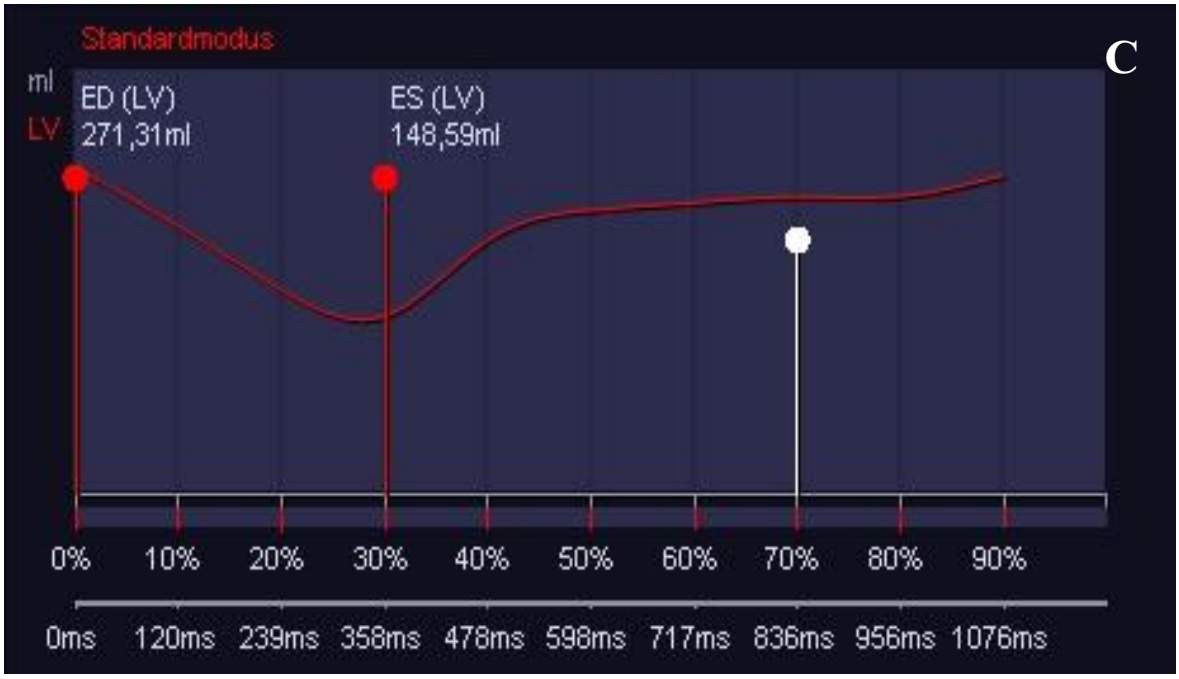

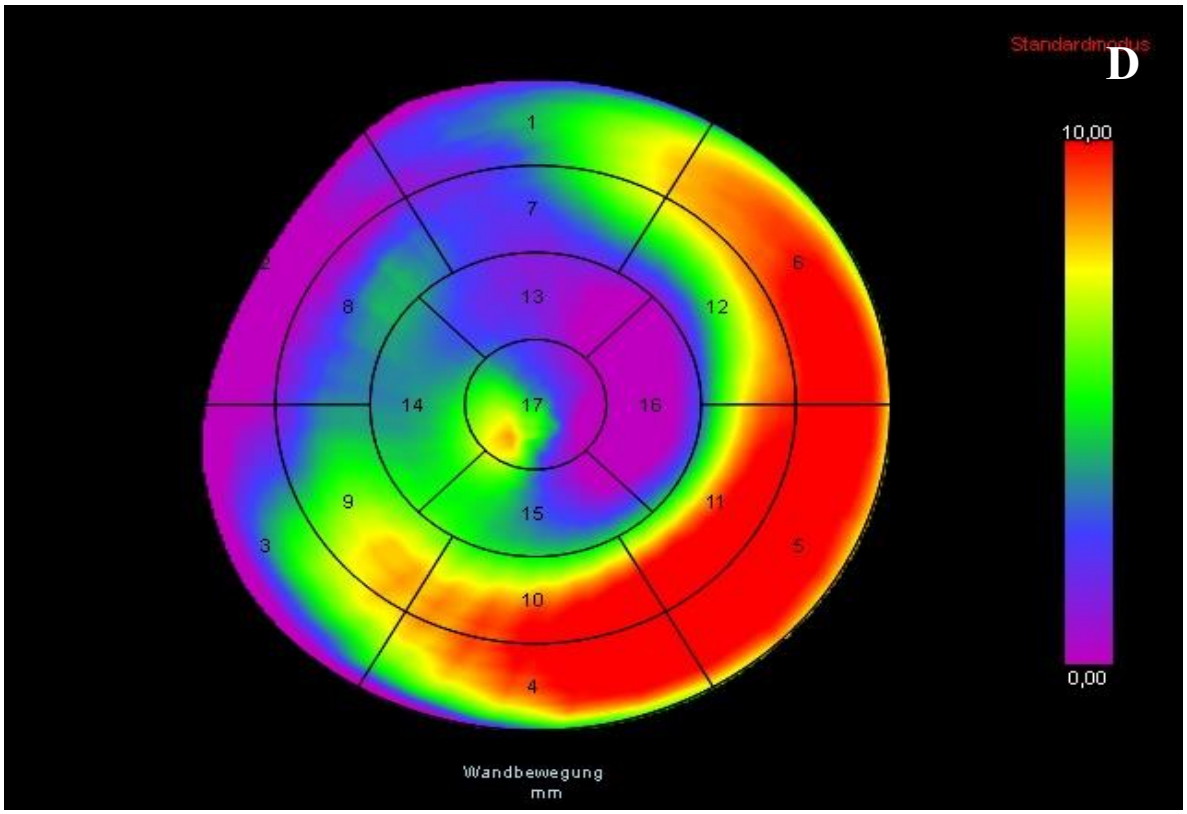

The left ventricular measurements were performed in a long-axis MPR 2-chamber view. The LV long axis length was defined as the distance between the mitral annulus geometrical center and the LV apex and was measured in systole and diastole (Figure 3).

Figure 3. Measurement of LV long-axis length in a 2-chamber view, reformatted images in diastole (A) and systole (B).

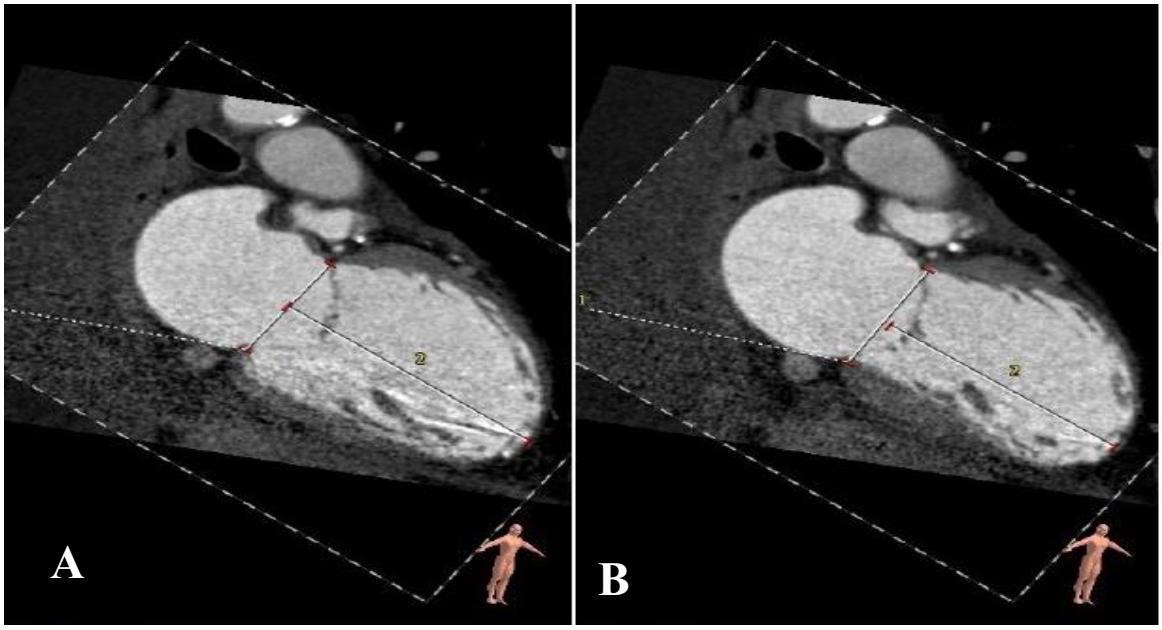

The systolic and diastolic LV volumetric sphericity index (SI) was calculated on the basis of the end-diastolic and end-systolic LV volume and LV long-axis length in a 2-chamber view according to the empirical formula (80):

$$SI = \text{LV volume}/\text{LV long axis}^{3} \times \pi/ 6.$$

The left atrial (LA) volume was measured by tracing the LA cavity area in end-systolic 2-chamber view (A1) and 4-chamber view (A2) reconstructions (Figure 4); the LA length (L) was calculated according to the simplified empirical formula (81):

$$(0.85xA1xA2)/L.$$

Figure 4. Tracing of LA cavity area in end-systolic 2-chamber view (A) and 4-chamber view (B) reconstructions.

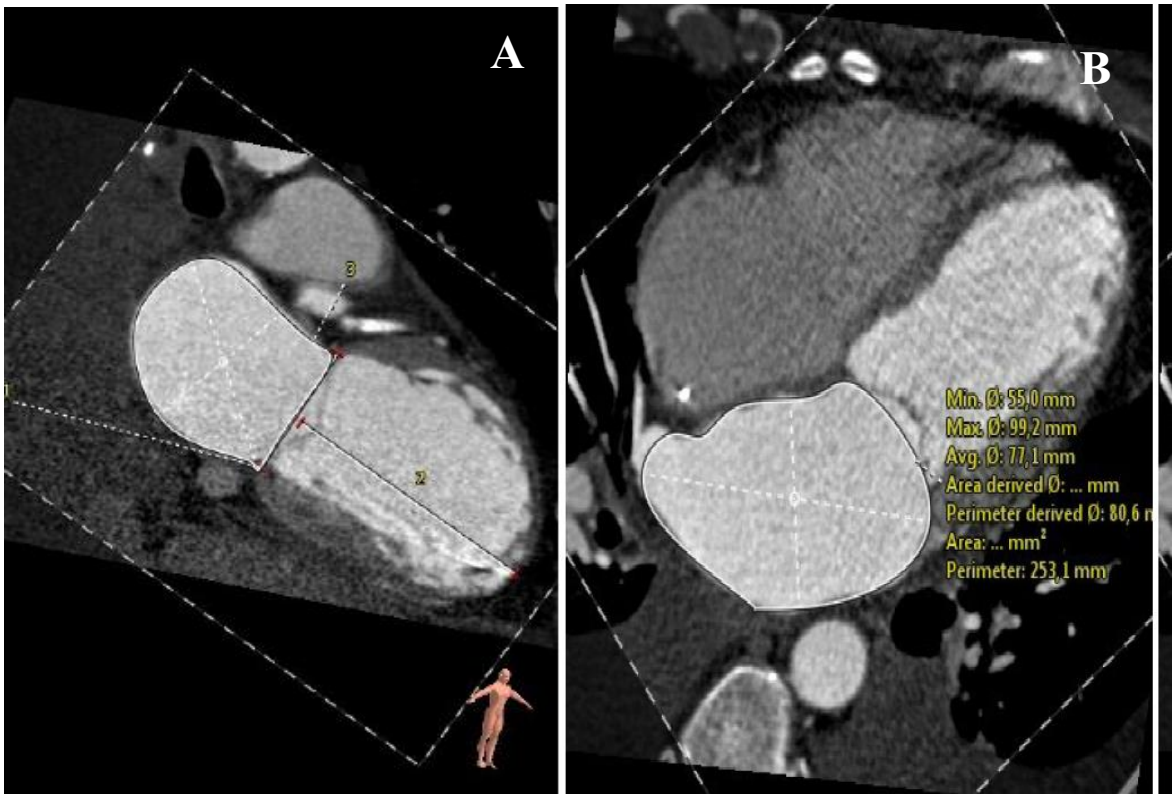

All parameters obtained were indexed to the body surface area (BSA).

All data were anonymized and transferred to a personal computer with the 3mensio structural heart software loaded on the desktop for a post-processing analysis of the MV complex. The 3mensio structural heart software package (8.0 module; Pie Medical Imaging, Netherlands) offers a dedicated workflow for mitral analysis by providing double-oblique multi-planar (MPR) and 3D reconstructions (82).

Using this software, a double-oblique MPR is computed such that two views are displayed. The mitral annulus was located on the short-axis MPR views by placing a landmark point. A second landmark was placed near the apex of the LV on the long-axis MPR view. By placing these two landmarks, the LV line was defined and adjusted if needed. To trace the mitral annulus, the long-axis MPR slices were rotated around the mitral-valve-to-apex axis and a view to start selecting the annulus was chosen. 16 data points were manually placed along the contour of the fibrous continuity while rotating the long-axis view by 22.5° in a stepwise fashion aligned to the left ventricular long axis. Each time a data point was placed, the long axis made a standard rotation, thus making it easier to place the next data point. After an initial segmentation of the saddle-shaped annulus, the annulus annotation was checked on the short-axis views and was corrected if

needed. The lateral and medial fibrous trigones were manually identified using the short- and long-axis views by scrolling through the images to obtain the most precise lateral and medial points of the attachment of the anterior leaflet. After finalizing the segmentation, parameters for the saddle-shaped annulus were derived automatically. The mitral annulus had a calculated center and two color-coded segments which were used to indicate the anterior and posterior side of the annulus. The trigones define the border between the anterior peak and posterior circumference (Figure 5).

Figure 5. Saddle-shaped MV annulus defined using 3mensio software (8.0 module; Pie Medical Imaging, Netherlands).

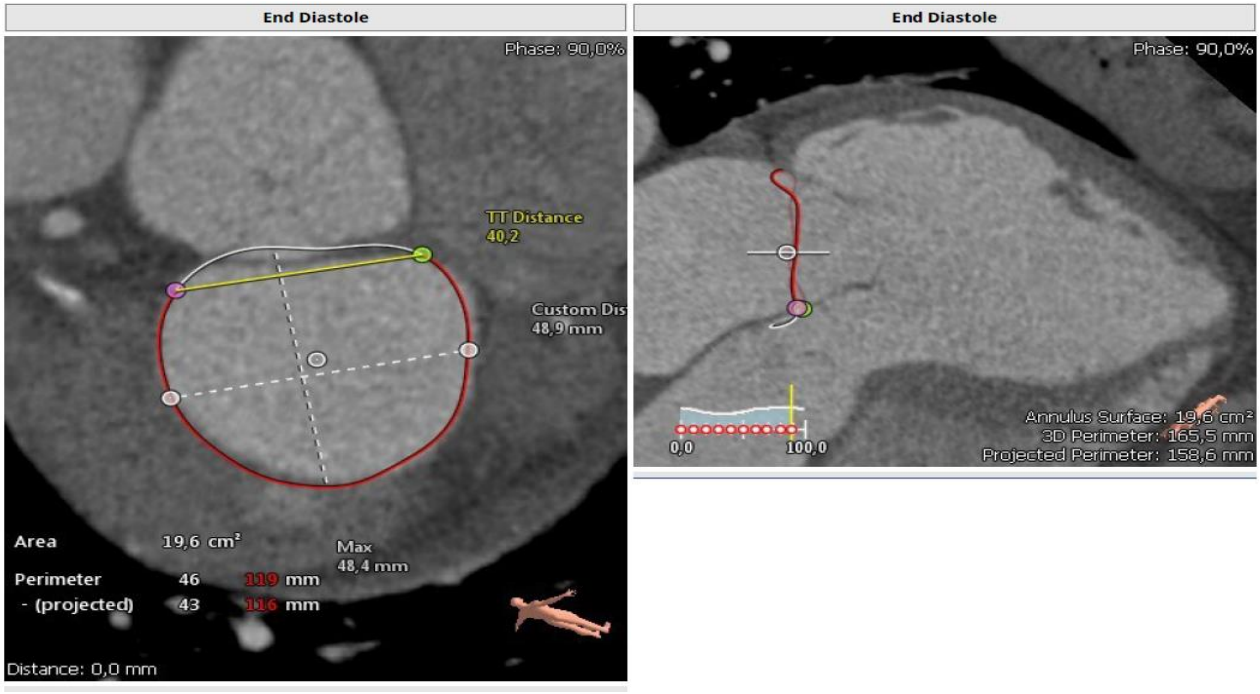

The saddle-shaped annulus includes the aortomitral continuity, whereas the D-shaped annulus is defined by being limited anteriorly by the trigone-to trigone distance, excluding the aortomitral continuity.

The annulus surface of the saddle-shaped annulus (As) is the area calculated when the annulus is projected to a plane perpendicular through the mathematical center of the annulus. The 3D perimeter of the saddle-shaped annulus (3D-Ps) is the entire circumference of the annulus as it exists in a 3D space. The 2D perimeter of the saddle-shaped annulus (2D-Ps) is the length of the annulus as it exists when projected to a plane perpendicular to the mathematical center. A virtual line connects the two trigones and is referred to as the trigone-to-trigone (TT) distance

(Figure 6). The septal-lateral (SL) distance for the saddle-shaped MV was defined as the projected distance from the aortic peak to the posterior peak.

The anterior and posterior 3D and 2D perimeters of the saddle-shaped annulus represent the length of the anterior and posterior aspects of the mitral annulus as it exists in a 3D and 2D space, respectively.

Figure 6. Saddle-shaped MV annular 3D segmentation and parameters in systole; the red line represents the posterior 3D perimeter; the white line represents the anterior 3D perimeter; the pink and green dots are trigones; the yellow line between them represents the TT distance. Short-axis view of the MA region (A) and 2-chamber view reformatted image (B).

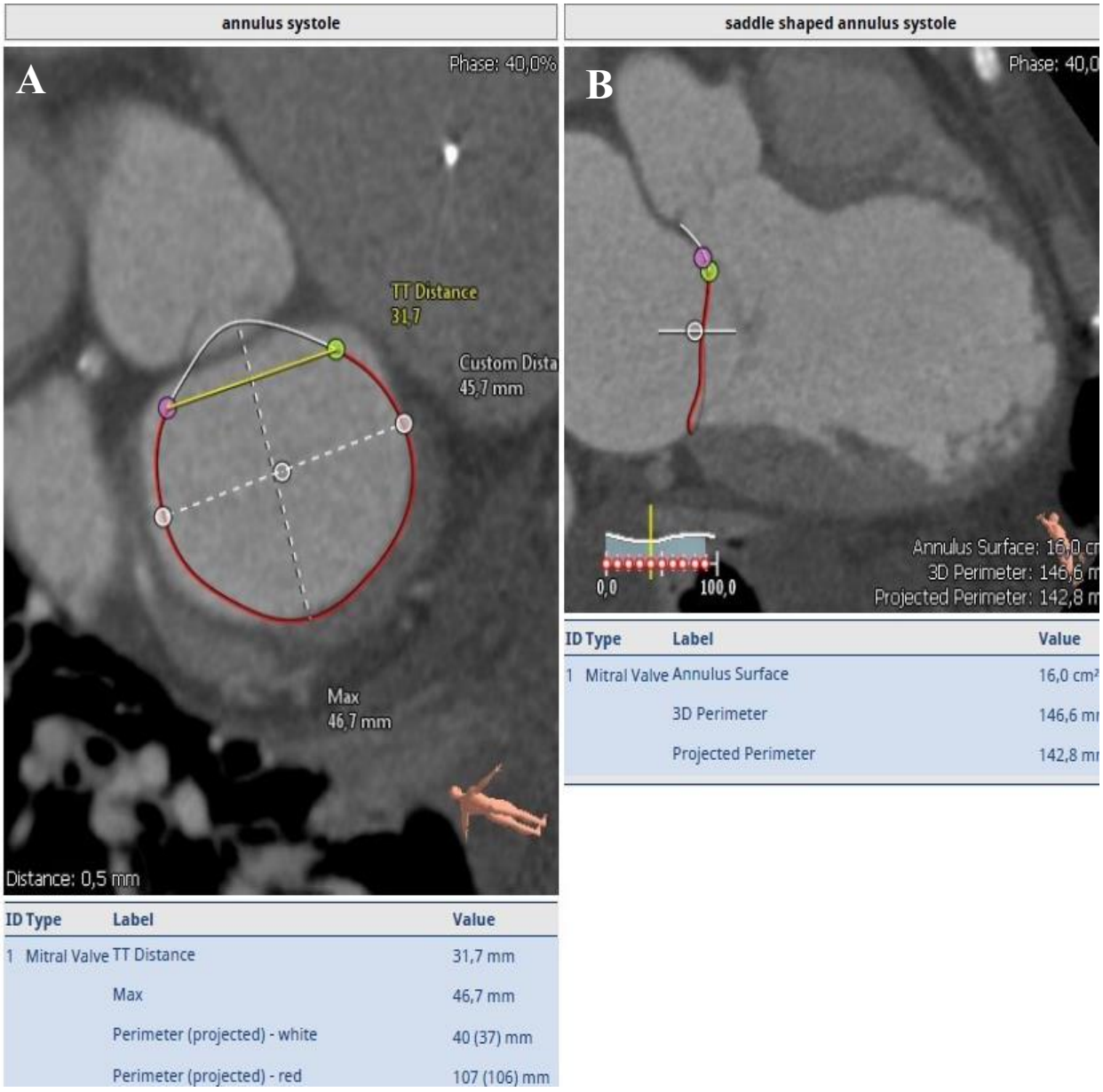

The annular height of the saddle-shaped annulus (Hs) was measured as the perpendicular distance between the highest peak and the lowest nadir of the 3D contour to the least squares plane. An example is given in Figure 7.

Figure 7. Saddle-shaped mitral annulus height measurement using 3mensio software. 2-chamber view reformatted image of the MV saddle-shaped annulus region (A); volume-rendered image of the MA (B); schematic views of the nonplanar saddle-shaped mitral annulus (C and D).

The red line represents the posterior 3D perimeter; the white line represents the anterior 3D perimeter; the pink and green dots are trigones.

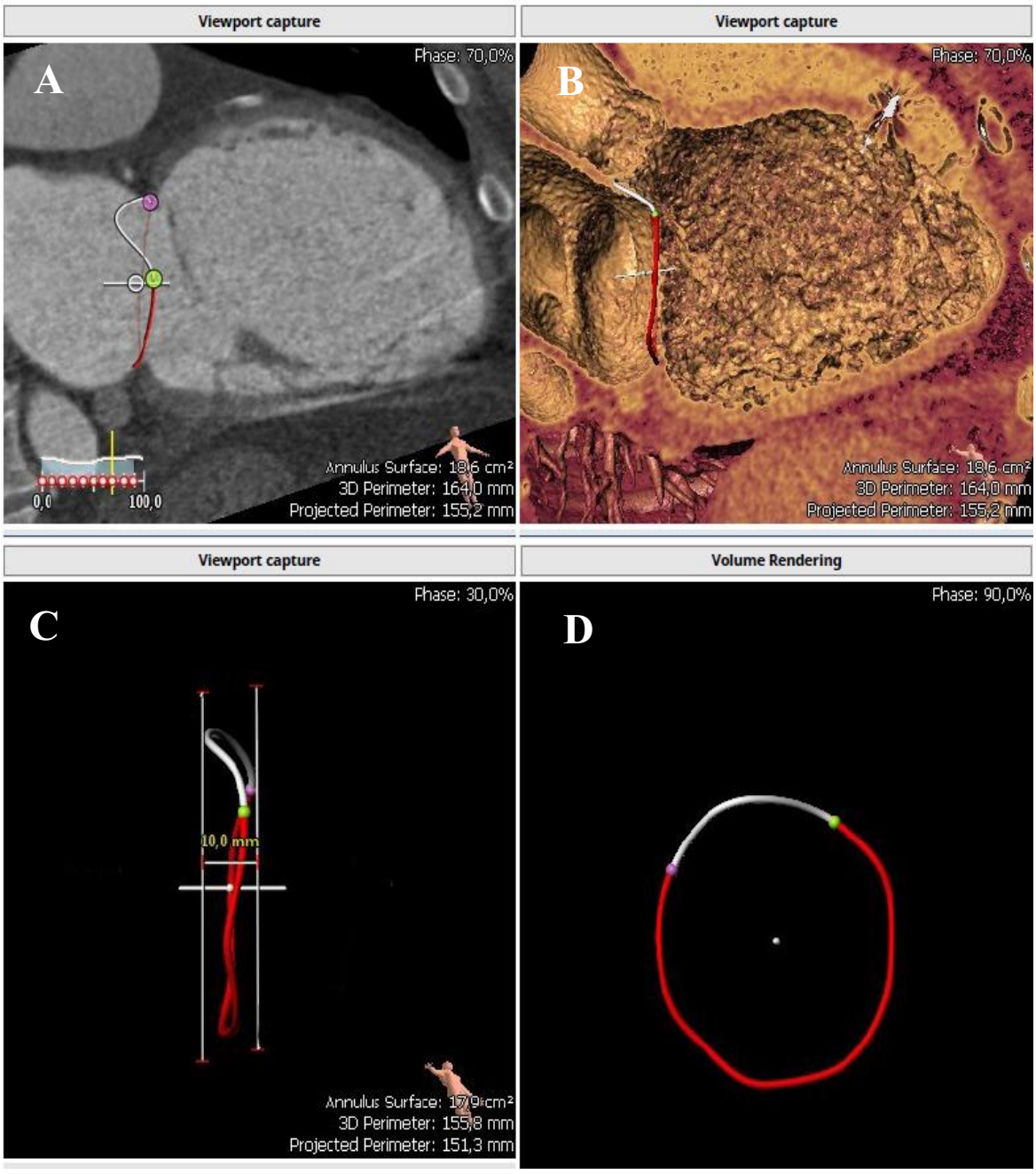

There is an automatic technique to unsaddle the anatomical mitral annulus. The anterior margin of the annulus for the D-shaped MV annulus was defined by the TT distance. The 3D perimeter (3D-Pd) is an annular circumference which is computed for the D-shaped annulus as the sum of the TT distance and the 3D circumference of the posterior aspect of the annulus. The 2D perimeter (2D-Pd) is the sum of the TT distance and the 2D circumference of the posterior aspect. The septal-lateral (SL) distance of the D-shaped annulus is a projected distance from the TT line to the posterior peak. An example of a D-shaped MA is shown in Figure 8.

Figure 8. Representative example of a D-shaped mitral annulus assessment.

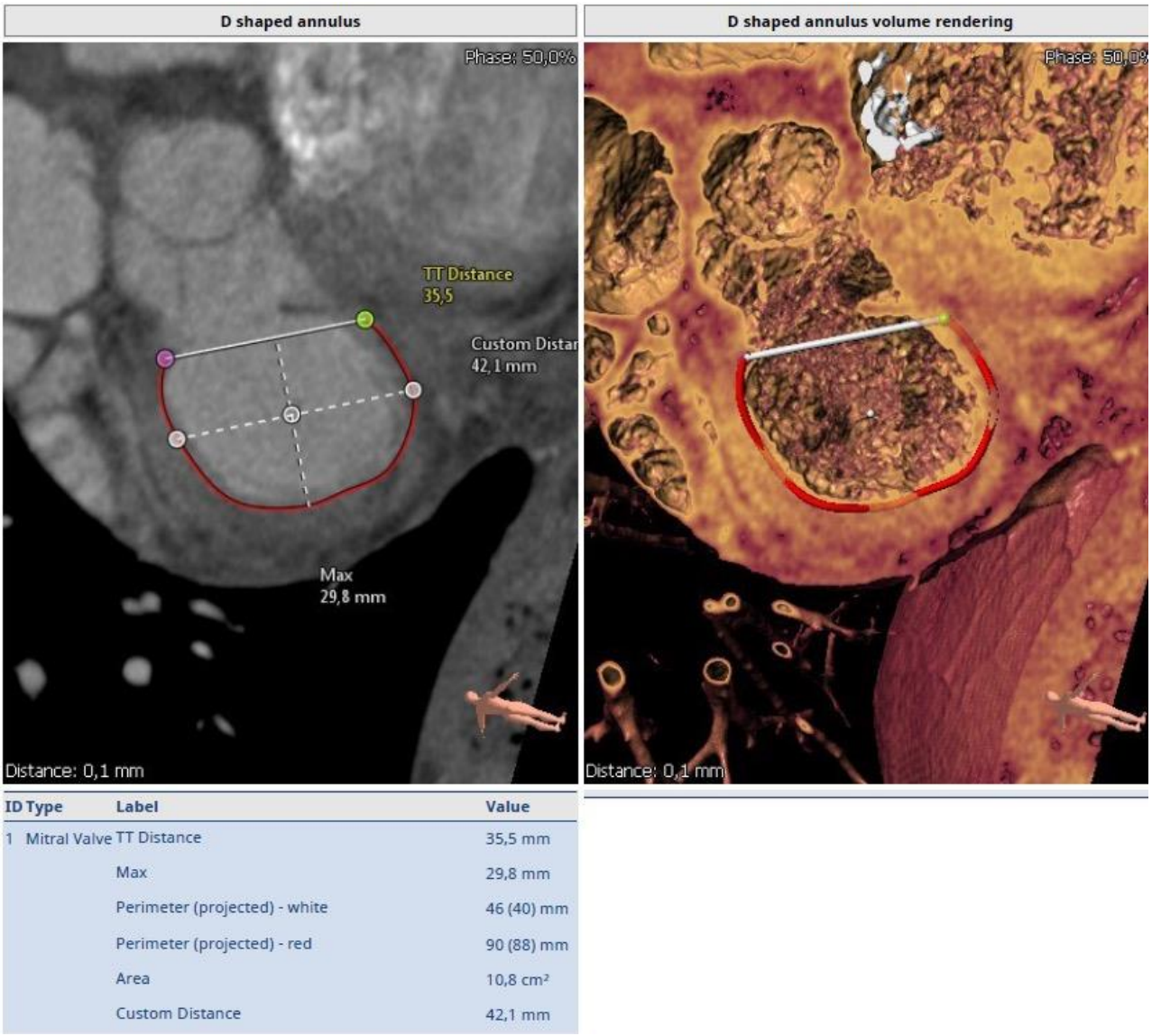

ID	Type	Label	Value
1	Mitral Valve	TT Distance	35,5 mm
		Max	29,8 mm
		Perimeter (projected) - white	46 (40) mm
		Perimeter (projected) - red	90 (88) mm
		Area	10,8 cm²
		Custom Distance	42,1 mm

The aorto-mitral angle is the angle between the MA trajectory and the LVOT long axis. It was measured automatically after defining the location of the aortic valve annulus by using markers identifying the nadirs of the three leaflets of the aortic valve (Figures 9, 10)

Figure 9. Aortic root 3 nadirs defined using the 3mensio software.

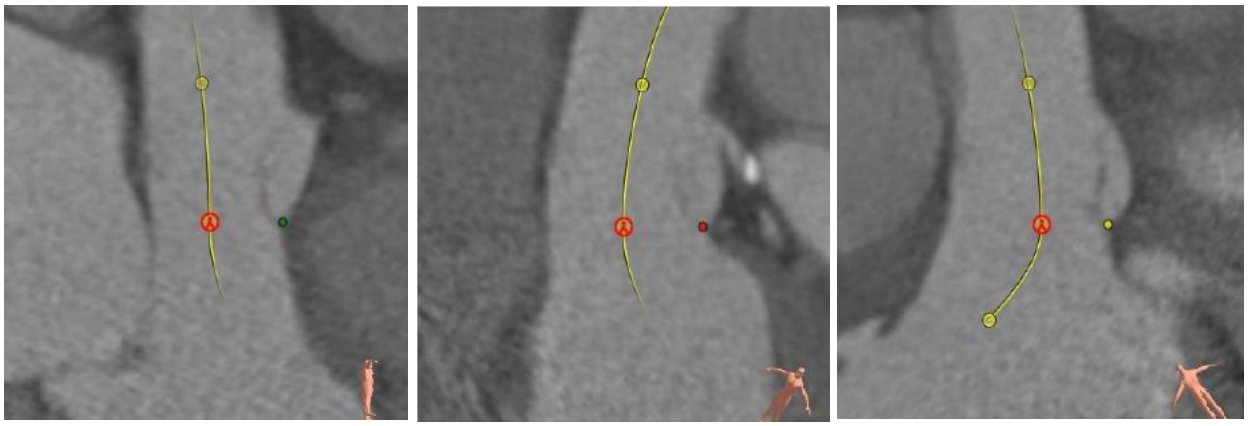

Figure 10. Measurement of the aorto-mitral angle. Multiplanar reformatted and volume-rendered images. Aortic nadirs in the short-axis aortic annulus view (A); aorto-mitral angle in a 3-chamber reformatted image (B) and in volume-rendered images (C and D).

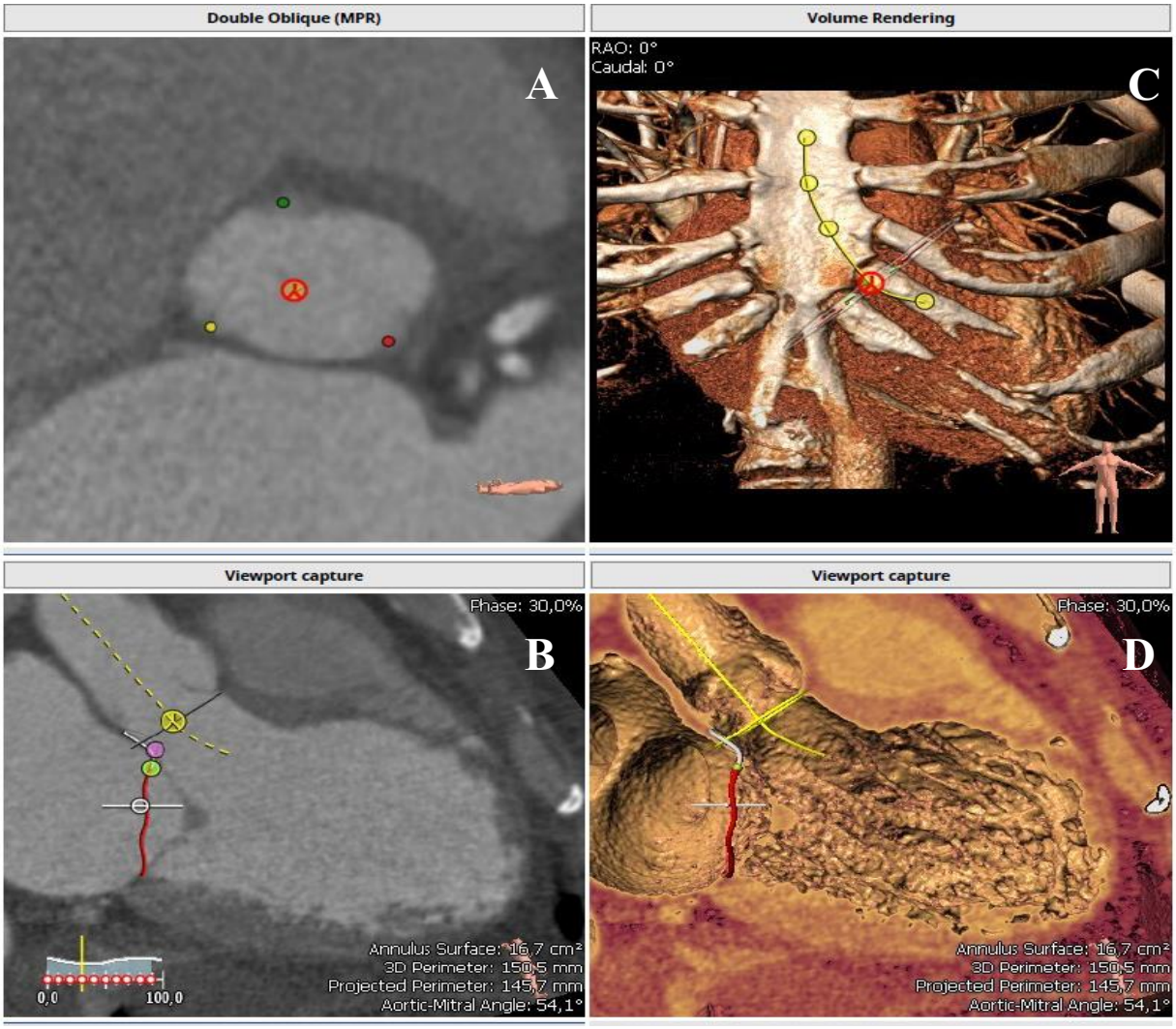

The LA-to-LV axis angle was defined using 3-chamber-view images in systole by manually placing the angle tool between them (Figure 11).

Figure 11. 3-chamber view reformatted image with angle tool for measuring the LA-to-LV axis placed on it.

The respective distances from the annulus to the anterior and posterior papillary muscles were defined in systole and diastole. There were measured by placing 3D markers on the head of the anterior and posterior papillary muscles nearest to the annulus and by defining the three-dimensional linear distance between the annulus and the actual 3D marker. The entire analysis took approximately one hour per patient (about 5 minutes for the assessment of each cardiac phase). Obtaining MV parameters and segmentation of the mitral annulus were successful in all subjects in all cardiac phases, despite the use of a radiation dose-reduction CT protocol. Most of the parameters were defined in all ten phases of the cardiac cycle to enable a dynamic assessment of the mitral valve. This minimum of measurements offers a detailed analysis of the size of the mitral apparatus, MV geometry, dynamics and mobility. The severity of corresponding mitral regurgitation in FMR group of patients was estimated by echocardiography prior to the CTA.

3.5. Statistical analysis

All data were analyzed using the statistical software IBM SPSS Statistics, Version 22 (Armonk, NY, IBM Corp.). Continuous variables were expressed as means ± SD (standard deviations) and categorical variables as frequencies and percentages. The Kolmogorov-Smirnoff test was used to test for a normal distribution of continuous variables. The Shapiro-Wilk Test was used to test for a normal distribution. The T-test was used to compare means for normally distributed variables. The Wilcoxon test was used to assess variables that did not exhibit a normal distribution between two groups (i.e. control group and with FMR). A P-value <0.05 was considered statistically significant.

4. RESULTS

4.1 Baseline characteristics

All parameters were analyzed for a total of 46 subjects who were divided into a control group (defined as healthy subjects; n=24) and an FMR group (n=22) as outlined in the study population section above. All patients in the FMR group had mitral valve regurgitation classified at least as grade II (by prior echocardiography). The first group consisted of 24 healthy subjects (18 male, 6 females; 47 ± 11 years; range: 24-70 years) who were referred for a CTA for coronary assessment. Coronary disease was excluded by CTA. The healthy subjects had no history of any cardiac disease, cardiac surgery or intervention. All of them had normal LV volumetric parameters, normal LV sphericity index and no LV wall motion abnormalities. Healthy subjects had not undergone prior cardiac surgery or intervention. The mean BMI for the first group was 26 ± 2.8 kg/m². The mean LVEF was 72 ± 6%. The second group consisted of 22 patients with FMR (15 male, 7 female; 63 ± 7 years; range: 50-75 years, BMI 26 ± 3.5 kg/m², LVEF 31 ± 9%).

Details of the demographic and baseline characteristics for both groups are provided in Table 1.

Table 1. Baseline characteristics and volumetric parameters of the study population

Variable	Group 1 (n=24)	Group (n=22)	P-value
Age, years	47 ± 11	63 ± 7	<0.0001
Gender, M/F	18/6	15/7	n/a
BMI, kg/m²	26 ± 2.8	26 ± 3.5	1
LVEDD, mm	55.2 ± 5.6	81± 11.2	<0.0001
LVEDV, ml	138.6±25.6	313.7±100.8	<0.0001
LVESV, ml	40.5±15.2	222.4±92.4	<0.0001
SV, ml	97.8±16. 7	91.3±22	0.2627
LVEF, %	71.5±5.8	31.2±9.3	<0.0001
LVEDVI, ml/qm	70.5±10.9	161.8±47.5	<0.0001
LVESVI, ml/qm	20.2±5.9	108±48.5	<0.0001
SVI, ml/qm	50.4±7.9	47.5±10.3	0.2874
CO, l/min	7.2±1.5	6.7±2	0.3401
CI, l/min/qm	3.7±0.8	3.5±0.9	0.4292
LV-sphericity index, systole	0.2±0.08	0.4±0.1	<0.0001
LV-sphericity index, diastole	0.3±0.07	0.5±0.1	<0.0001
LA volume, end systole, ml	79.9±18.9	157.2±46.6	<0.0001
LA volume index, ml/qm	41±9.9	81±19.8	<0.0001

BMI = body mass index; LVEDD = end-diastolic diameter of LV; LVEDV / LVESV = left ventricular end-diastolic / systolic volume; SV = stroke volume; LVEF = LV ejection fraction; LVEDVI, LVESVI = left ventricular end-diastolic / systolic volume index; SVI = stroke volume index; CO = cardiac output; CI = cardiac index; LA = left atrium.

Values are expressed as the mean ± SD. M indicates male, F indicates female.

4.2 Systolic and diastolic LV sphericity index

Measurements of the LV volumetric sphericity index (SI) showed a significant difference between the two groups. The mean diastolic LV volumetric sphericity index (SI) is 0.3 ± 0.07 versus 0.5 ± 0.09 in diastole and 0.16 ± 0.08 versus 0.44 ± 0.1 in systole (P <0.05) with no significant difference between the diastolic and systolic values in the FMR group (Figure 12).

Figure 12. LV sphericity index values in diastole (a) and in systole (b) for both groups

Fig. 12a. Fig. 12b.

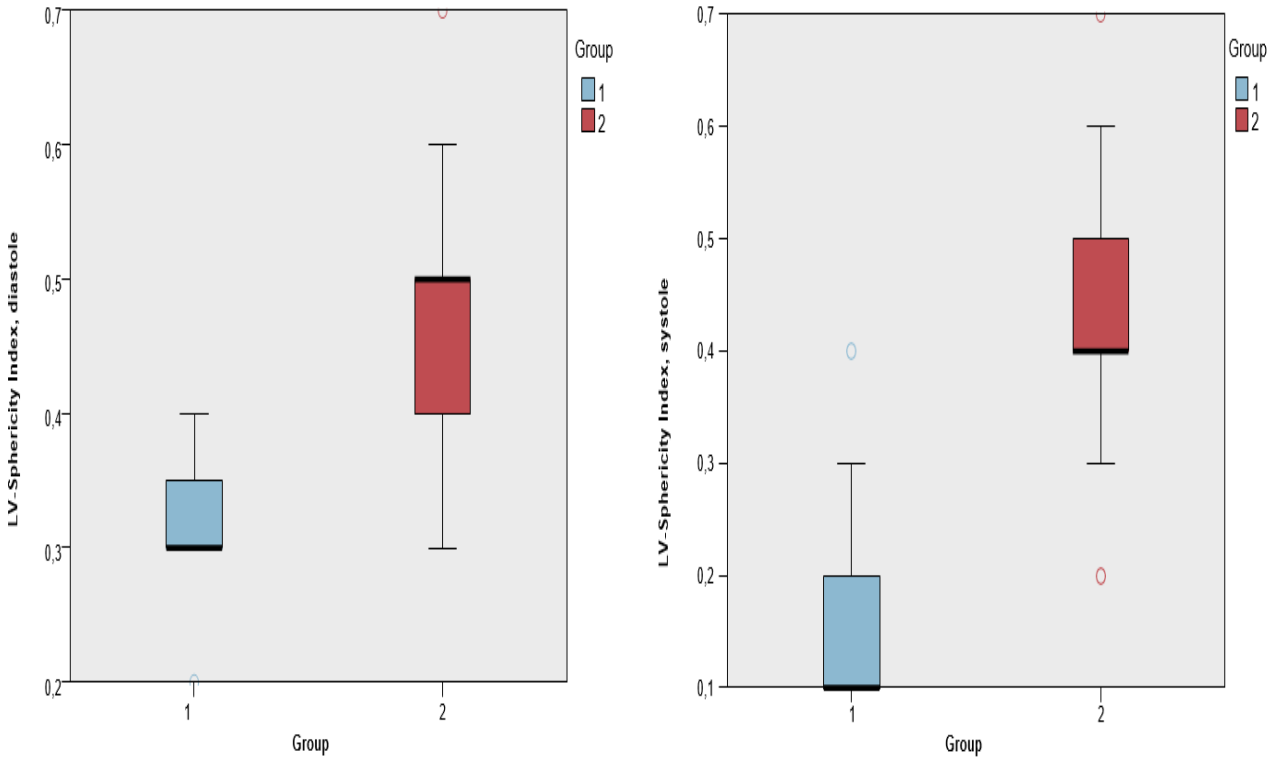

4.3 Mitral annulus dimensions

The annular contours were successfully segmented in all patients. All annulus parameters are expressed as means calculated from the values of the MV parameters in all subjects in each group and were averaged over all 10% phases of the cardiac cycle.

The average mean area of the mitral valve (annulus surface) in FMR patients for saddle-shaped and D-shaped models was 14.6 ± 0.52 cm² and 12.7 ± 0.49 cm², respectively, and was found to be higher than those of the control group (12.1 ± 2.2 cm² vs. 10.3 ± 1.6 cm²). The average mean 3D perimeter (the entire circumference of the annulus as it exists in a 3D space) of the saddle-shaped annulus (3D-Ps) was 130.8 ± 10.8 mm vs. 143 ±2.7 mm in Group 1 and Group 2, respectively. The 2D perimeter of the saddle-shaped annulus (2D-Ps) was also greater in Group 2 compared to healthy subjects (136.7 ±2.4 mm [Group 2] vs. 124.8 ± 10.3 mm [Group 1]). The 3D and 2D perimeters of the D-shaped MA values were without a significant difference between both groups and with minor differences between the 3D and 2D values in the FMR group (121.5 ± 8.1 mm vs. 132.5 ± 2.7 mm for 3D-Pd, and 119.9 ± 9.1 mm vs. 131.2 ± 2.5 mm for 2D-Pd).

The difference between the trigone-to trigone (TT) distance between the two groups was not pronounced and was 33.7 ± 1.9 mm in the control group and 34.6 ± 1.4 mm in the FMR group. The septal-lateral (SL) distance for the saddle-shaped MV was defined as 36.64 ± 5.7 mm for Group 1 and 43 ± 1.3 mm for Group 2. The septal-lateral (SL) distance for the D-shaped MV was defined as 29.3 ± 5.7 mm for Group 1 and 34.7 ± 1.4 mm for Group 2.

4.3.1 Mitral annulus dimensions in the saddle-shaped model

The saddle-shaped MA dimensions, including annulus surface, entire circumference, projected circumference etc., were generally found to be significantly larger in the FMR group compared to the healthy subjects. Tables 2-7 contain a summary of annulus surface (As), projected circumference of the entire saddle-shaped annulus (2D-Ps), entire anterior circumference (3D-Ps anterior), entire posterior circumference (3D-Ps posterior), projected distance from the aortic peak to the posterior peak (SLs), projected anterior circumference (2D-Ps anterior), projected posterior circumference (2D-Ps posterior) and annular height (Hs). The fluctuation in MA dimensions throughout the cardiac cycle was found to be significantly higher in Group 1 (healthy subjects) than in Group 2.

The graph showing the mean values of the mitral annulus entire circumference for the saddle-shaped annulus model is a good example of minor changes in the MA dimensions during the cardiac cycle in the FMR group (Figure 13). Difference in the mitral annulus height for the saddle-shaped annulus (Hs) and fluctuations thereof during the cardiac cycle is shown on another graph (Figure 14).

Table 2. Annulus surface (As) values in the S-shaped mitral annulus model for both groups

Annulus surface (As)	Group 1		Group 2		
	Mean	SDV	Mean	SDV	p-value
Mitral valve saddle-shaped annulus surface, cm² 0%	10.50	1.98	14.32	2.12	<0.0001
Mitral valve saddle-shaped annulus surface, cm² 10%	11.48	1.69	14.66	2.22	<0.0001
Mitral valve saddle-shaped annulus surface, cm² 20%	12.53	1.84	14.73	2.39	0.001
Mitral valve saddle-shaped annulus surface, cm² 30%	12.61	2.12	14.84	2.44	0.002

Mitral valve saddle-shaped annulus surface, cm² 40%	12.51	2.08	14.54	2.25	0.003
Mitral valve saddle-shaped annulus surface, cm² 50%	12.49	1.96	14.67	2.30	0.001
Mitral valve saddle-shaped annulus surface, cm² 60%	12.39	1.79	14.51	2.15	0.001
Mitral valve saddle-shaped annulus surface, cm² 70%	12.29	1.84	14.58	2.42	0.001
Mitral valve saddle-shaped annulus surface, cm² 80%	12.45	1.72	14.65	2.20	0.001
Mitral valve saddle-shaped annulus surface, cm² 90%	11.81	2.09	14.83	2.17	<0.0001

Figure 13. Difference in the mitral annulus entire circumference for the saddle-shaped annulus (3D-Ps)

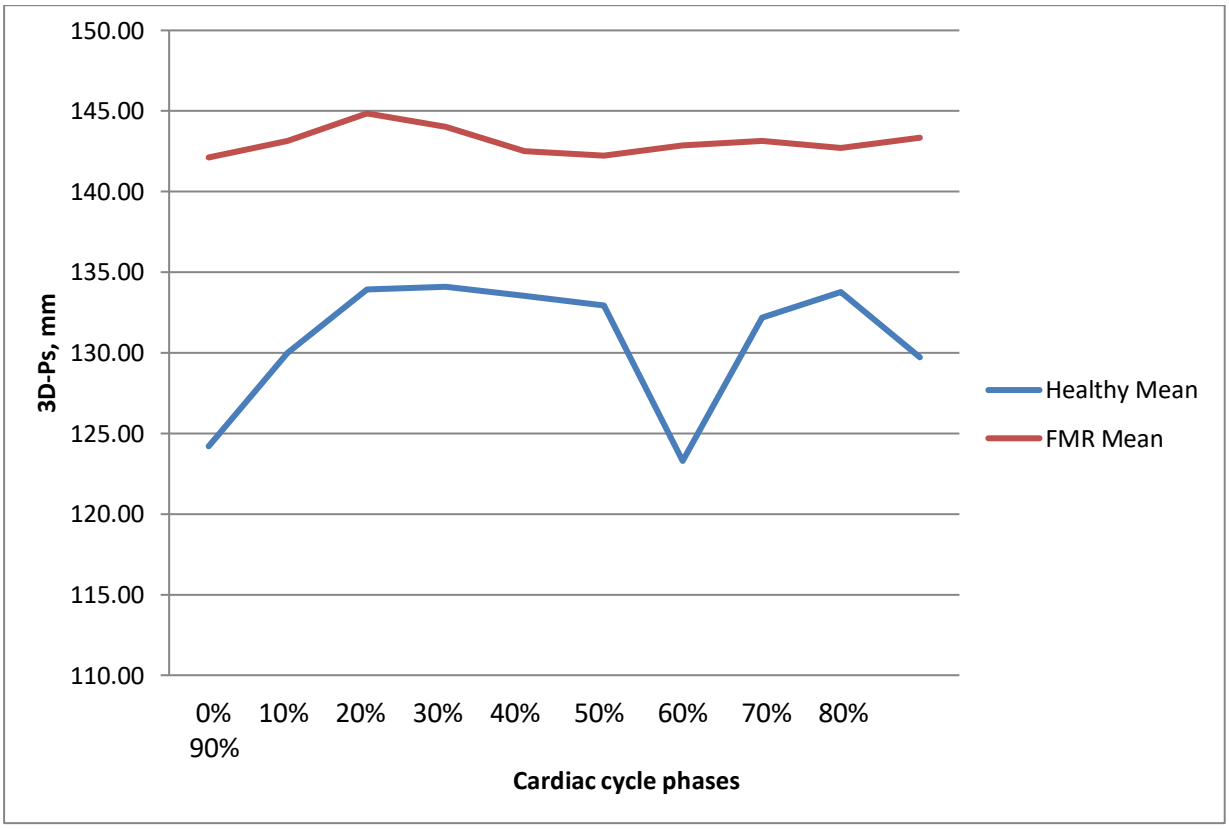

Table 4. Projected circumference of the entire saddle-shaped annulus (2D-Ps) for both groups in all phases of the cardiac cycle

Projected circumference of the entire saddle-shaped annulus (2D-Ps)	Group 1		Group 2		
	Mean	SDV	Mean	SDV	p-value
2D-Ps circumference, mm, 0%	116.79	10.83	135.22	10.09	<0.0001
2D-Ps circumference, mm, 10%	121.83	8.96	136.60	10.09	<0.0001
2D-Ps circumference, mm, 20%	127.09	9.60	137.21	11.11	0.002
2D-Ps circumference, mm, 30%	127.02	10.62	137.60	11.01	0.002
2D-Ps circumference, mm, 40%	126.40	10.42	136.19	10.65	0.003
2D-Ps circumference, mm, 50%	126.65	9.71	136.90	10.69	0.002
2D-Ps circumference, mm, 60%	126.49	8.88	136.36	9.93	0.001
2D-Ps circumference, mm, 70%	126.12	9.18	136.53	11.38	0.002
2D-Ps circumference, mm, 80%	126.68	8.68	136.93	9.98	0.001
2D-Ps circumference, mm, 90%	123.42	10.91	137.39	9.86	<0.0001

Table 5. Summary of the projected distance from the aortic peak to the posterior peak (SLs)

Projected distance from the aortic peak to the posterior peak (SLs)	Group 1		Group 2		
	Mean	SDV	Mean	SDV	p-value
SL from the aortic peak to the posterior peak, 0%	32.89	3.09	42.63	3.66	<0.0001
SL from the aortic peak to the posterior peak, 10%	34.83	2.94	42.12	4.22	<0.0001
SL from the aortic peak to the posterior peak, 20%	37.36	3.04	42.84	4.16	<0.0001
SL from the aortic peak to the posterior peak, 30%	37.93	2.86	43.11	3.87	<0.0001

SL from the aortic peak to the posterior peak, 40%	38.60	2.98	43.42	3.48	<0.0001
SL from the aortic peak to the posterior peak, 50%	37.97	3.36	42.91	3.91	<0.0001
SL from the aortic peak to the posterior peak, 60%	37.53	3.25	43.35	3.67	<0.0001
SL from the aortic peak to the posterior peak, 70%	37.23	2.80	43.30	4.29	<0.0001
SL from the aortic peak to the posterior peak, 80%	37.03	2.68	43.29	3.47	<0.0001
SL from the aortic peak to the posterior peak, 90%	35.03	3.42	43.26	3.76	<0.0001

Table 6. Summary of the entire anterior circumference (3D-Ps anterior) of the MA for both groups

Entire anterior circumference (3D-Ps anterior)	Group 1		Group 2		
	Mean	SDV	Mean	SDV	p-value
3D-Ps anterior, mm, 0%	41.25	4.61	44.55	4.32	0.02
3D-Ps anterior, mm, 10%	43.33	4.57	45.23	3.79	0.13
3D-Ps anterior, mm, 20%	43.83	3.51	46.64	4.69	0.03
3D-Ps anterior, mm, 30%	44.54	4.92	46.55	6.15	0.23
3D-Ps anterior, mm, 40%	44.42	5.69	45.32	5.47	0.59
3D-Ps anterior, mm, 50%	44.00	4.11	44.45	5.30	0.75
3D-Ps anterior, mm, 60%	43.75	4.53	45.32	5.76	0.31
3D-Ps anterior, mm, 70%	43.83	4.31	50.77	16.79	0.07
3D-Ps anterior, mm, 80%	44.58	5.44	44.77	3.68	0.89
3D-Ps anterior, mm, 90%	41.88	3,5547	43.50	9.07	0.18

Table 7. Summary of the entire posterior circumference (3D-Ps posterior) of the MA for both groups

Entire posterior circumference (3D-Ps posterior)	Group 1		Group 2		
	Mean	SDV	Mean	SDV	p-value
3D-Ps posterior, mm,0%	82.88	8.65	98.05	8.38	<0.0001
3D-Ps posterior, mm, 10%	86.71	7.69	98.45	9.00	<0.0001
3D-Ps posterior, mm, 20%	90.08	8.89	98.14	9.67	0.005
3D-Ps posterior, mm, 30%	89.50	9.66	93.00	20.38	0.469
3D-Ps posterior, mm, 40%	89.08	9.26	97.23	9.82	0.006
3D-Ps posterior, mm, 50%	89.00	7.98	97.50	10.00	0.003
3D-Ps posterior, mm, 60%	90.21	9.18	97.55	9.09	0.009
3D-Ps posterior, mm, 70%	88.29	7.30	91.95	20.22	0.429
3D-Ps posterior, mm, 80%	89.13	6.92	97.77	9.45	0.001
3D-Ps posterior, mm, 90%	87.79	8.99	99.68	9.00	<0.0001

Table 8. Summary of the projected anterior circumference (2D-Ps anterior) of the MA

Projected anterior circumference (2D – Ps anterior)	Group 1		Group 2		
	Mean	SDV	Mean	SDV	p-value
2D-Ps anterior, mm, 0%	36.67	4.15	39.00	4.05	0.005
2D-Ps anterior, mm, 10%	37.92	4.19	40.14	3.24	<0.0001
2D-Ps anterior, mm, 20%	38.96	3.25	41.14	3.55	0.006
2D-Ps anterior, mm, 30%	39.63	4.66	42.09	5.10	0.003
2D-Ps anterior, mm, 40%	39.63	4.35	40.73	4.28	0.005
2D-Ps anterior, mm, 50%	39.79	3.45	41.00	4.20	0.002

2D-Psanterior, mm, 60%	38.63	3.27	40.59	4.34	0.003
2D-Ps anterior, mm, 70%	39.67	3.74	46.00	17.90	0.263
2D-Ps anterior, mm, 80%	39.46	3.54	41.18	3.70	0.001
2D-Ps anterior, mm, 90%	38.08	3.27	39.55	3.97	<0.0001

Table 9. Projected posterior circumference (2D-Ps posterior) for both groups

Projected posterior circumference (2D-Ps posterior)	Group 1		Group 2		
	Mean	SDV	Mean	SDV	p-value
2D-Ps posterior, mm,0%	80.00	7.95	96.14	8.15	0.06
2D-Ps posterior, mm, 10%	83.92	8.22	96.50	8.94	0.05
2D-Ps posterior, mm, 20%	88.17	8.97	95.95	9.43	0.04
2D-Ps posterior, mm, 30%	87.38	9.41	95.68	8.82	0.10
2D-Ps posterior, mm, 40%	87.13	9.40	95.55	9.90	0.39
2D-Ps posterior, mm, 50%	87.08	7.78	95.77	9.67	0.29
2D-Ps posterior, mm, 60%	87.88	8.08	95.68	8.85	0.09
2D-Ps posterior, mm, 70%	86.33	7.70	91.08	18.05	0.12
2D-Ps posterior, mm, 80%	87.29	7.15	96.23	9.31	0.11
2D-Ps posterior, mm, 90%	85.29	8.79	97.91	8.71	0.18

The annular height values in the saddle-shaped MA (were found to be not significantly different between the two groups, however there were fluctuations throughout the entire cardiac cycle for both groups.

The minimal and maximal annular height values (saddle-shaped model) in the first group were 9.99 ± 1.33 and 11.30 ± 1.74 and in the second group 10.24 ± 1.40 and 11.42 ± 2.35, respectively (Table 10).

Figure 14. Difference in the mitral annulus height for the saddle-shaped annulus (Hs) and fluctuations thereof during the cardiac cycle

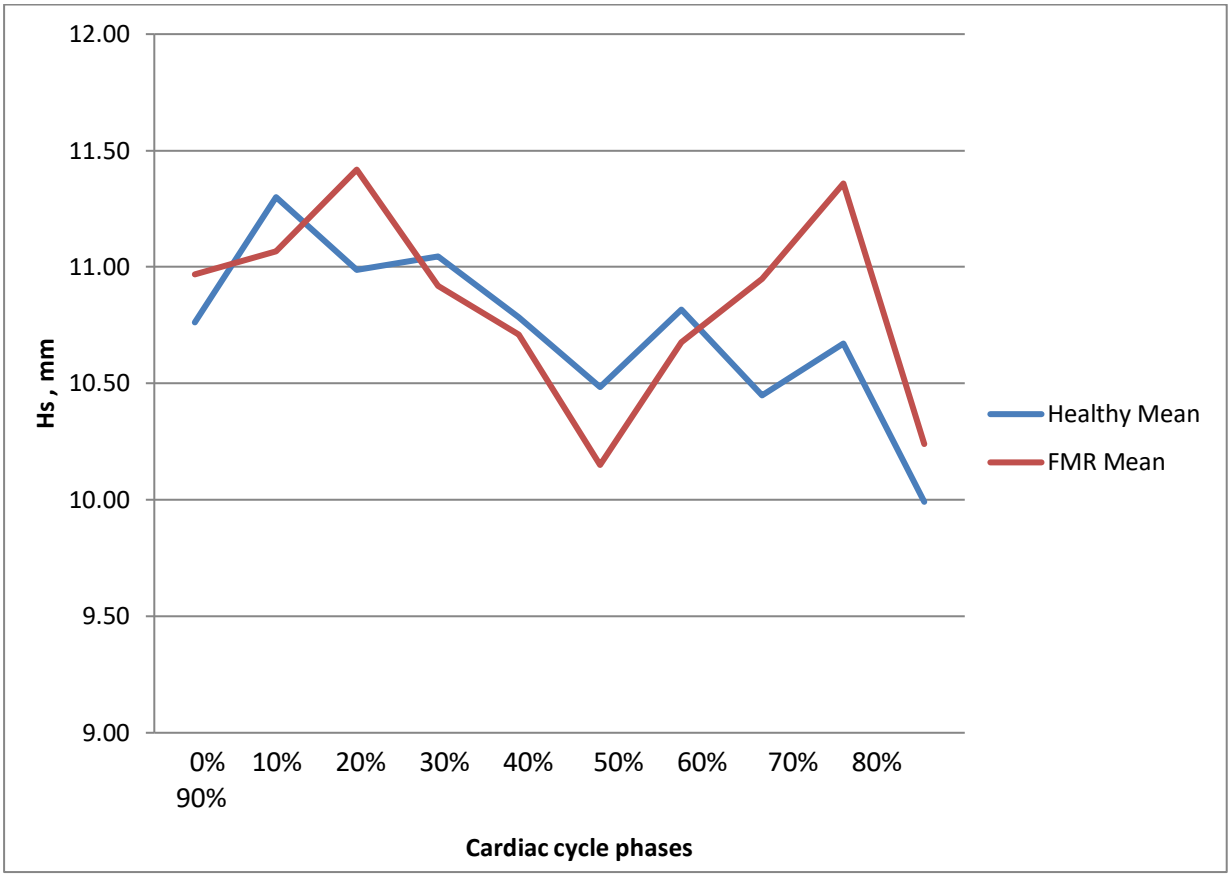

4.3.2. Mitral annulus dimensions in the D-shaped model

The D-shaped MA dimensions, including annulus surface (Ad), entire circumference (3D-Pd), projected distance from the aortic peak to the posterior peak in the D-shaped mitral annulus model (SLd), projected circumference and anterior circumference - which was defined as the trigone-to-trigone (TT) distance - were generally found to be significantly smaller in the first group compared to the second group; this trend was steady throughout the entire cardiac cycle. Tables 11-13 contain a summary of the results for some of the D-shaped mitral annulus parameters.

In addition, on graphs with mean values of mitral annulus entire circumference (3D-Pd) and projected circumference (2D-Pd) for D-shaped annulus model is obvious a continuous discrepancy between parameters in two groups (Figures 15, 16).

Table 11. Summary of mitral annulus surface dimensions in the D-shaped MA model (Ad) for every 10% phase of the cardiac cycle

Annulus surface (Ad)	Group 1		Group 2		
	Mean	SDV	Mean	SDV	p-value
Mitral valve, D-shaped annulus, Ad, cm², 0%	9.11	1.80	12.58	1.99	<0.0001
Mitral valve, D-shaped annulus, Ad, cm², 10%	9.92	1.72	12.78	2.08	<0.0001
Mitral valve, D-shaped annulus, Ad, cm², 20%	10.75	1.87	12.74	2.24	<0.0001
Mitral valve, D-shaped annulus, Ad, cm², 30%	10.71	2.12	12.67	2.20	0.004
Mitral valve, D-shaped annulus, Ad, cm², 40%	10.63	2.03	12.51	2.34	0.006
Mitral valve, D-shaped annulus, Ad, cm², 50%	10.65	1.82	12.62	2.27	0.002
Mitral valve, D-shaped annulus, Ad, cm², 60%	10.70	1.88	12.59	2.08	0.003
Mitral valve, D-shaped annulus, Ad, cm², 70%	10.51	1.80	12.65	2.37	0.001
Mitral valve, D-shaped annulus, Ad, cm², 80%	10.71	1.65	12.71	2.27	0.002
Mitral valve, D-shaped annulus, Ad, cm², 90%	10.27	1.98	13.00	2.08	<0.0001

Figure 15. Summary of dimensions of the mitral annulus entire circumference of the D-shaped annulus (3D-Pd) for every 10% phase of the cardiac cycle

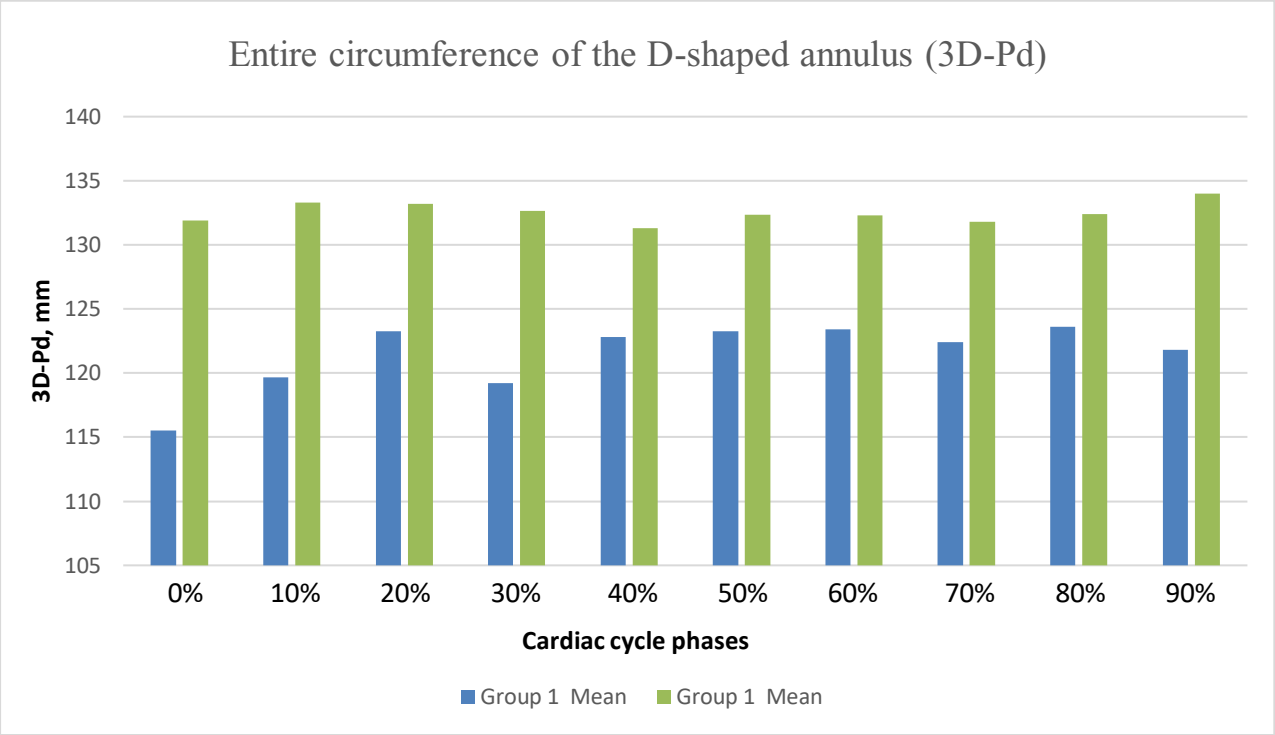

Figure 16. Projected circumference of the D-shaped annulus

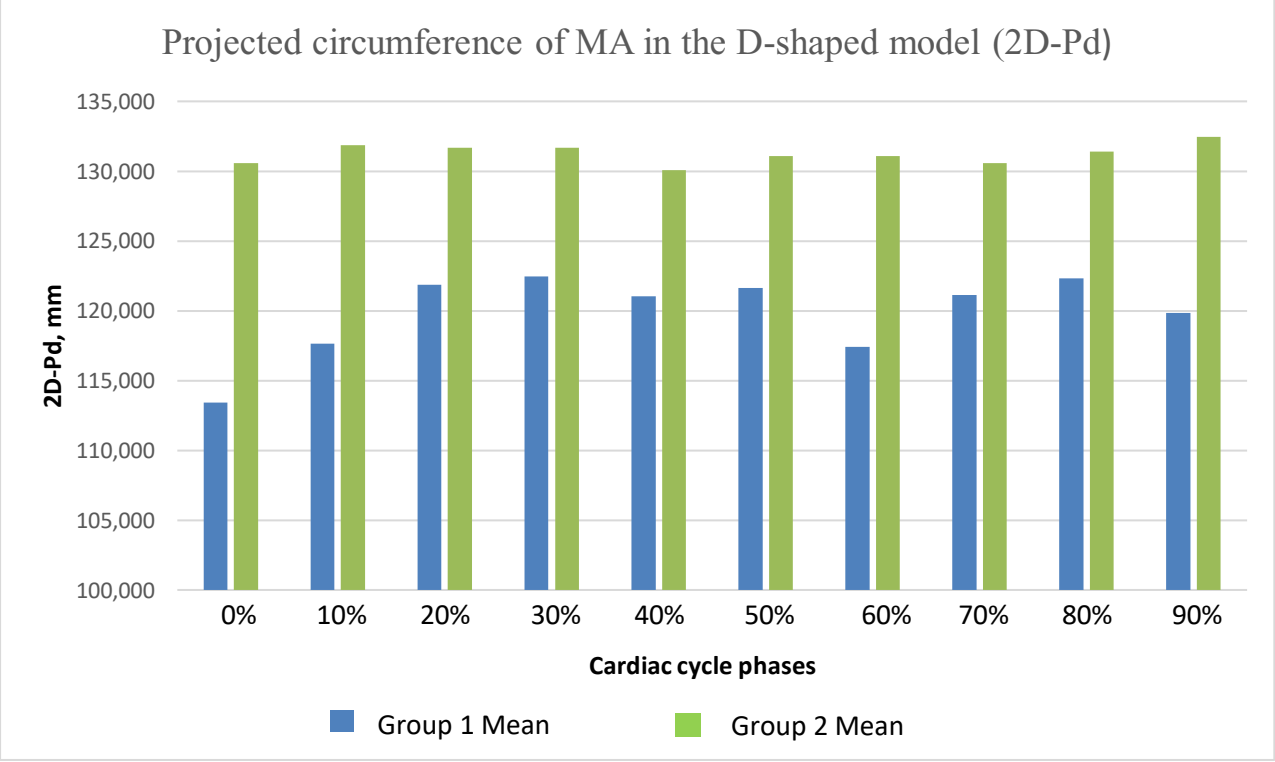

Table 12. Projected distance from the aortic peak to the posterior peak in the D-shaped mitral annulus model (SLd)

Projected distance from the aortic peak to the posterior peak in the D-shaped mitral annulus model (SLd)	Group 1		Group 2		
	Mean	SDV	Mean	SDV	p-value
SLd, mm, 0%	26.58	2.71	35.04	3.33	<0.0001
SLd, mm, 10%	27.95	2.87	34.47	3.60	<0.0001
SLd, mm, 20%	29.52	2.99	34.40	3.66	<0.0001
SLd, mm, 30%	32.26	12.35	34.05	3.25	0.498
SLd, mm, 40%	29.33	4.98	34.34	3.60	<0.0001
SLd, mm, 50%	29.78	2.83	34.42	3.89	<0.0001
SLd, mm, 60%	29.80	3.50	34.83	3.88	<0.0001
SLd, mm, 70%	29.41	3.04	35.04	3.80	<0.0001
SLd, mm, 80%	29.53	3.02	35.15	3.66	<0.0001
SLd, mm, 90%	28.69	3.63	35.40	3.49	<0.0001

Table 13. Trigone-to-trigone (TT) distance representing the anterior border of the MA in the D-shaped model

Trigone-to-trigone (TT) distance	Group 1		Group 2		
	Mean	SDV	Mean	SDV	p-value
TT distance, mm 0%	32.54	3.77	33.89	3.20	0.196
TT distance, mm, 10%	33.19	2.95	34.83	2.64	0.054
TT distance, mm, 20%	33.64	2.69	35.09	2.80	0.082
TT distance, mm, 30%	34.33	3.80	35.31	3.46	0.365
TT distance, mm, 40%	33.65	3.21	34.10	3.14	0.630
TT distance, mm, 50%	34.05	3.24	34.84	3.24	0.413
TT distance, mm, 60%	33.24	2.72	34.72	3.48	0.118
TT distance, mm, 70%	34.14	3.32	34.07	3.43	0.942
TT distance, mm, 80%	34.44	3.17	34.67	3.17	0.803
TT distance, mm, 90%	34.01	3.09	34.31	3.31	0.748

4.3.2 Comparison of the two mitral annulus models and between the 2D and 3D dimensions

When comparing the two mitral annulus models, parameters including the annulus area, 3D and 2D perimeter (especially the anterior one) and the SL distance values were larger for the saddle-shaped model due to including the aorto-mitral continuity. This tendency is similar in both groups, but shows a large gap in the range in Group 1. For the saddle-shaped annulus the average mean area throughout the cardiac cycle was 12.1 ± 2.1 cm² (range: 10.5-12.61) for the control group and 14.6 ± 0.52 cm² (range: 14.32-14.84) for the FMR patients. Compared to the area of the D-shaped annulus (10.3 ± 1.6 cm² (range: 9.4-10.8) vs. 12.7 ± 0.5 cm² (range: 12.5-13), respectively, the average mean area of the saddle-shaped annulus was thus considerably larger. The discrepancy between the mean 3D circumferences of the saddle-shaped and the D-shaped model is more pronounced than in 2D circumference values of both MA models. The 3D perimeter of the saddle-shaped annulus (3D-Ps) was 130.8 ± 10.8 mm (range: 123.3-134.1) in Group 1 vs. 143 ± 2.7 mm (range: 142.1-144.9) in Group 2. The 3D perimeter of the D-shaped annulus in Group 1 was 121.5 ± 8.1 mm (range: 115.5-123.6) vs. 132.5 ± 2.7 mm (range: 131.3-133.98) in Group 2. The 2D-Ps was 124.8 ± 10.3 mm (range: 116.8-127.1) in healthy subjects vs. 136.7 ±2.4 mm (range: 135.2-137.6) in FMR patients. The 2D-Pd values were 119.9 ± 9.1 mm (range: 113.4-122.5) vs. 131.2 ± 2.5 mm (range: 130-132.5) for Groups 1 and 2, respectively. Likewise, there was notable difference between the anterior 3D and 2D perimeter of the saddle-shaped annulus values, whereas there were only slight changes between them in D-shaped model and minor changes between the 3D and 2D posterior perimeter values in both models. The anterior 3D perimeter of the saddle-shaped annulus for both groups was 43.5 ± 3.3 mm vs. 45.7 ± 7.3 mm, and the posterior 3D perimeter was 88.3 ± 7.3 mm vs. 96.9 ± 7.7 mm, respectively. The anterior 2D perimeter of the saddle-shaped annulus for both groups was 28.5 ± 3.1 mm vs. 41.1 ± 7 mm, and the posterior 2D perimeter was 86 ± 8.1 mm vs. 95.6 ± 6.8 mm, respectively. Compared with the D-shaped model, the SL distance in the saddle-shaped model was significantly longer (mean SLs 36.6 ± 5.7 mm [range: 32.9-38.6] in the control group and 43 ± 1.3 mm [range: 42.1-43.4] in the FMR group; mean SLd 29.3 ± 5.7 mm [range: 26.6-32.3] in Group 1 and 34.7 ± 1.35 mm [range: 34-35.4] in Group 2). The mean TT distance remained constant for both MA models. As the above values clearly show, the differences in the 3D and 2D entire perimeter, the anterior and posterior circumference and the SL distance were more pronounced in the saddle-shaped model and not very significant in the D-shaped model. Moreover, the gap between the 3D and 2D parameters for both MA assessment models is greater in Group 1 than in Group 2.

4.3.3. Comparison of MA parameters in systole and diastole between the two groups

There were statistically significant differences in mitral annulus dimensions, MA to papillary muscle distances and other parameters in systole and diastole between the healthy subjects and the FMR group (Figure 17). Most of the parameters were higher in the second group compared to the healthy subjects. For example, the saddle-shaped annulus area in systole was 12.575 ± 2 cm² vs. 14.732 ± 2.5 cm² and in diastole 11.646 ± 2.2 cm² vs. 14.655 ± 2.3 cm² for Groups 1 and 2, respectively. However, the gap between most of the values in systole and diastole is greater in Group 1 than in Group 2, where the difference between the values in systole and diastole is not as pronounced.

Figure 17. Mean values of MA dimensions for saddle-shaped and D- shaped approaches in systole and diastole

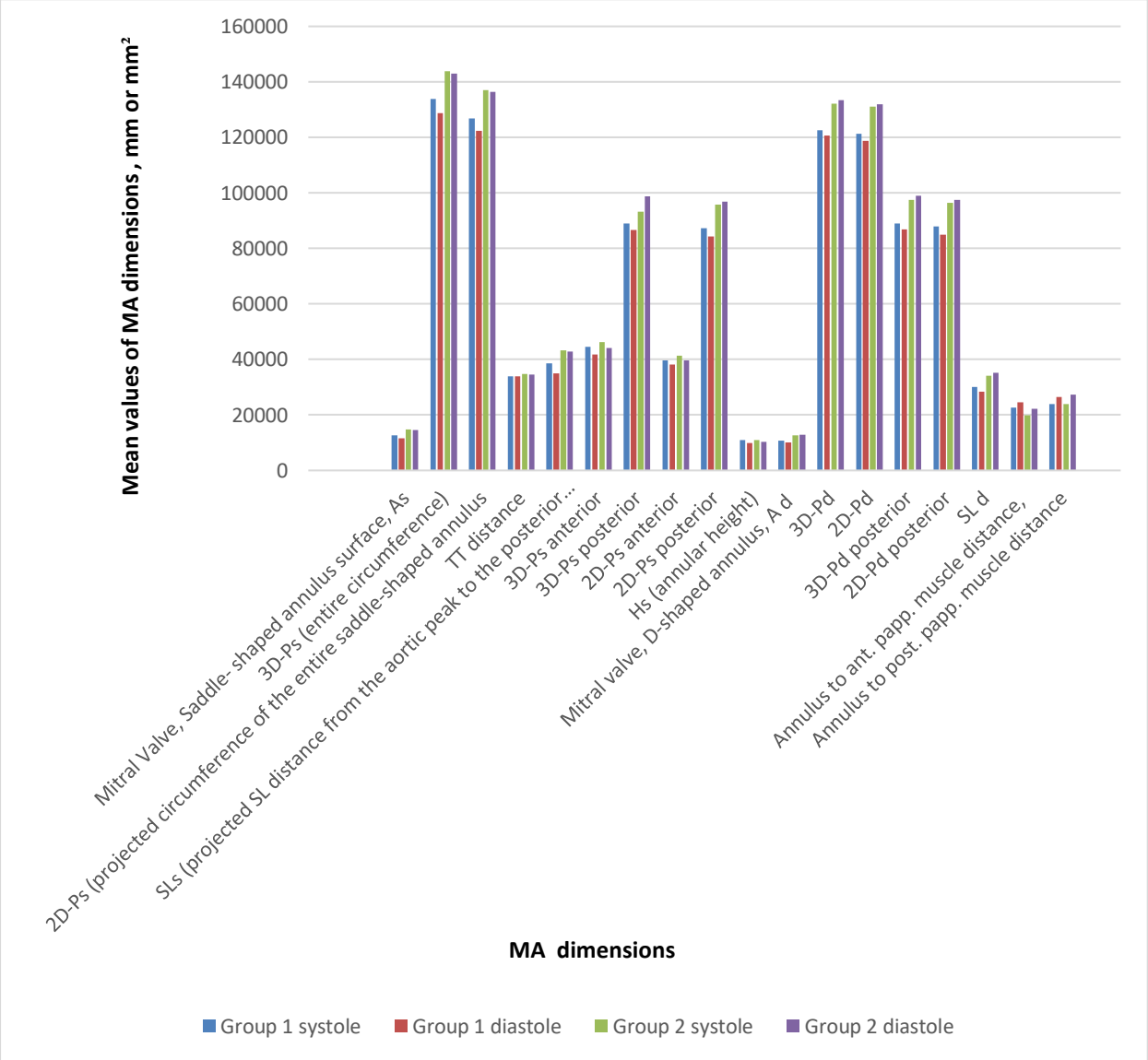

4.4 Aorto-mitral angle

The aorto-mitral angle was measured for the saddle shaped MV annulus in every 10% phase of the cardiac cycle. The measurements values were higher in the healthy group and this pattern remained consistent through the entire cardiac cycle. This means that the aorto-mitral angle was steeper in Group 2. The maximal mean aorto-mitral angle degree value in the first group was 58.5 ± 5.91 ($P < 0.001$) in 40% phase of cardiac cycle and minimal mean value was 51.59 ± 6.22 (P 0.001) in 90% phase of cardiac cycle. In the second group the maximal and minimal mean aorto-mitral angle degree value were 48.94 ± 7.07 (in 50% phase of cardiac cycle) and 42.16 ± 7.22 (in 0% phase of cardiac cycle), respectively. A difference of AMAA values for both groups is illustrated in Figure 18.

Figure 18. Mean values of the aorto-mitral angle for both groups.

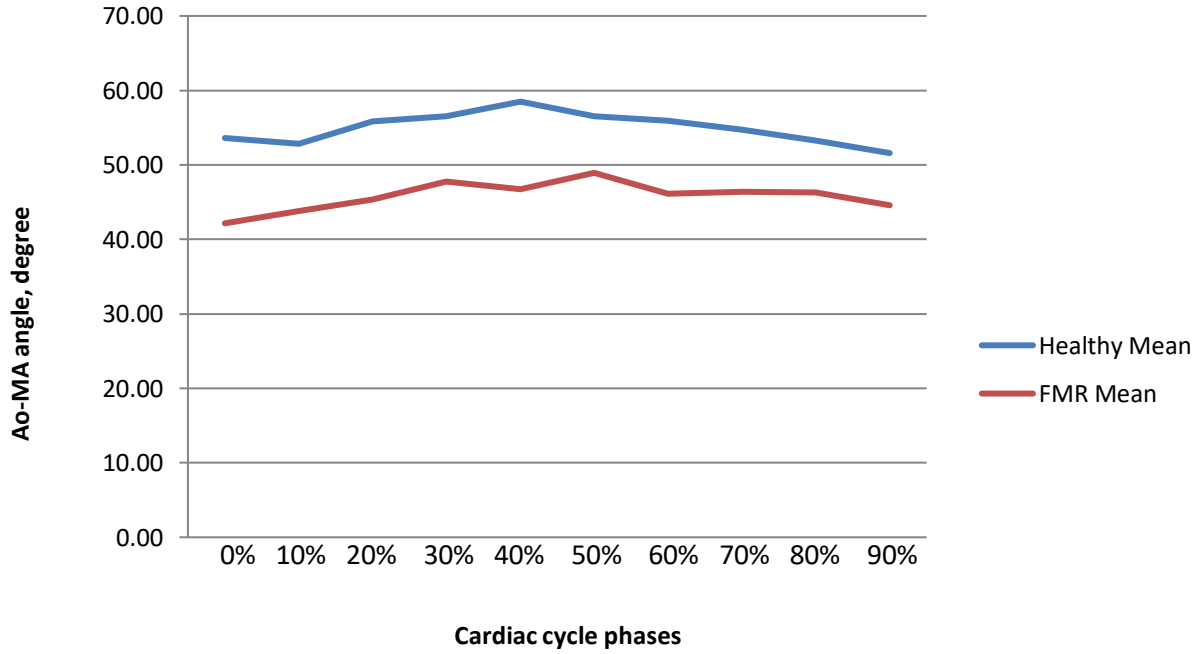

4.5 Annulus to papillary muscles distances

The distances for the mitral annulus to the anterior and posterior papillary muscle heads were measured in systole and diastole in all subjects and averaged ≥20 mm.

The difference in the distance between the MV annulus and the anterior papillary muscle is evident between the two groups. The mean annulus to anterior PM distance in systole was 22.7 ± 3.9 mm in the first group and 19.8 ± 3.2 mm in the second group (p-value 0.0207) and, in diastole, 24.6 ± 4.2 mm versus 22.1 ± 3.4 mm (p-value 0.0341), respectively. There was no big difference in the mean distance of the MV annulus to the posterior PM between the two groups.

Based on conventional criteria, the difference in the mean distance between the mitral annulus and the posterior PM is considered to be not statistically significant at 23.9 ± 3.9 mm vs. 24 ± 4.4 mm (p-value 0.9360) in systole and 26.5 ± 4.2 mm vs. 27.2 ± 4 mm (p-value 0.5703) in diastole.

4.4. LA-to-LV axis angle

The LA-to-LV angle was measured in the 3-chamber view during the systolic cardiac phase.
No significant difference was found between the average LA-to-LV angle in the healthy subjects and in the patients with FMR. The mean LA-to-LV axis angle was 151 ± 6.4° (range: 138-164) and 157.5 ± 6.4° (range: 146-168), respectively (Figure 19).

Figure 19. Difference in LA-to-LV axis angle during systole in the 3-chamber view (reformatted images) between healthy subjects (Group 1) and patients with FMR (Group 2)

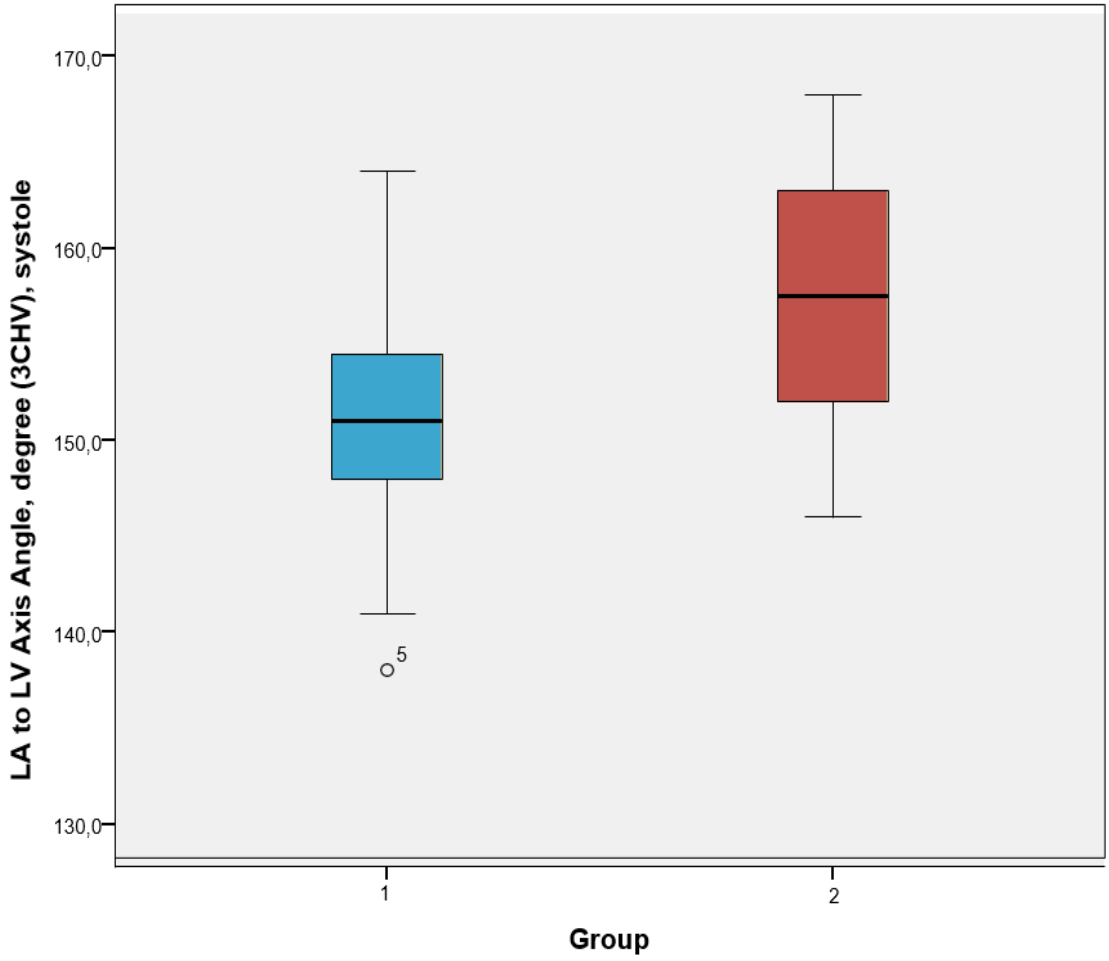

4.5 Mitral annular dynamics (mobility of the MA)

The mobility of the mitral annulus was defined as the difference between the minimum and maximum of each parameter. Means and standard deviations were calculated to compare the mobility. As shown in the table and exemplary graphs, the mobility of the MV annulus in healthy subjects is consistently higher than in second group.

The summary of the mean values of the mobility of the mitral annulus throughout the cardiac cycle for the control and FMR groups are shown in Table 15 and Figures 20 and 21.

Table 15. Mean values of the mitral annulus mobility (mean ±SD)

Parameter	Mean annulus mobility		P-value
	Group 1	Group 2	
3D-mitral annular circumference (mm)	17 ± 7.4	11 ± 3.9	< 0.05
2D-mitral annular circumference (mm)	15 ± 4.4	8 ± 3	< 0.001
Trigone-to-trigone distance (mm)	6 ± 1.9	5 ± 1	0.06
Antero-posterior-distance 3D (SL distance) (mm)	8 ± 2.2	5 ± 1.9	< 0.001
Aorto-mitral annular angle (°)	15 ± 6.2	12 ± 3.9	1

Figure 20. MA mobility: Anteroposterior-distances (SLs-distance 3D) for both groups in all cardiac cycle phases (the orange line represents the minimum for each patient, the blue line the maximum for each patient).

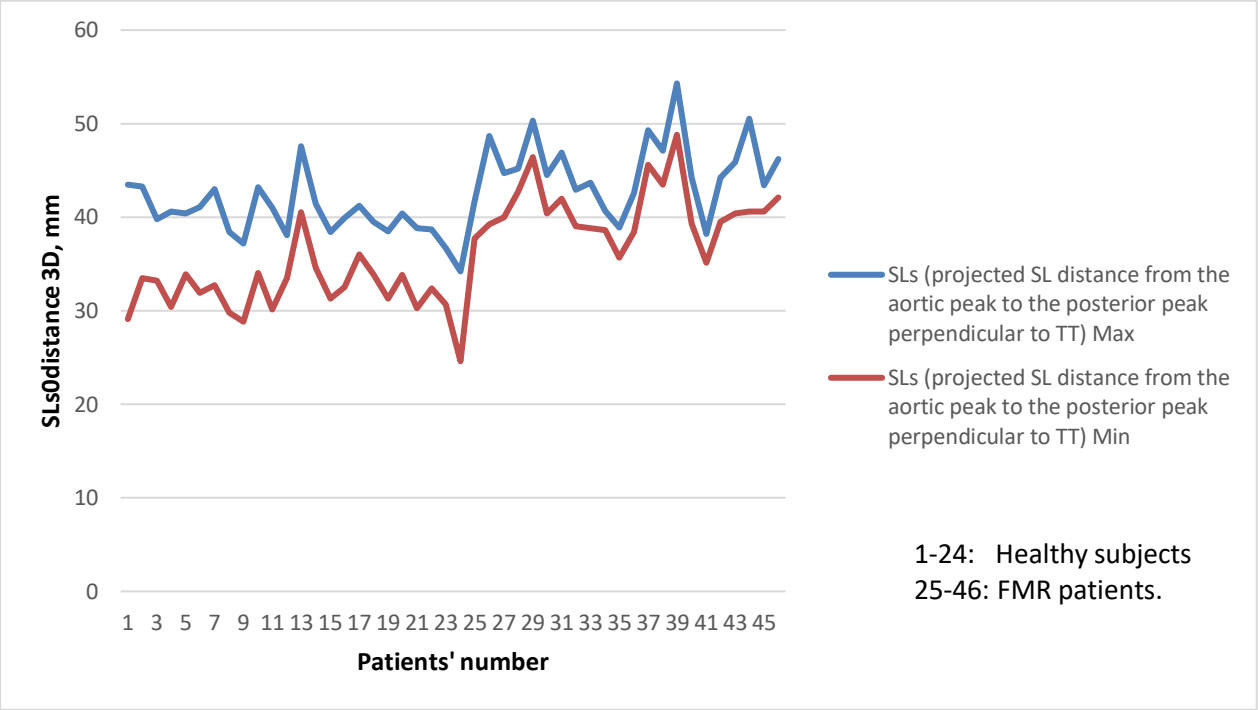

Figure 21. MA mobility: 3D entire circumference for the saddle-shaped annulus (3D-Ps) for both groups in all cardiac cycle phases (the orange line represents the minimum for each patient, the blue line the maximum for each patient).

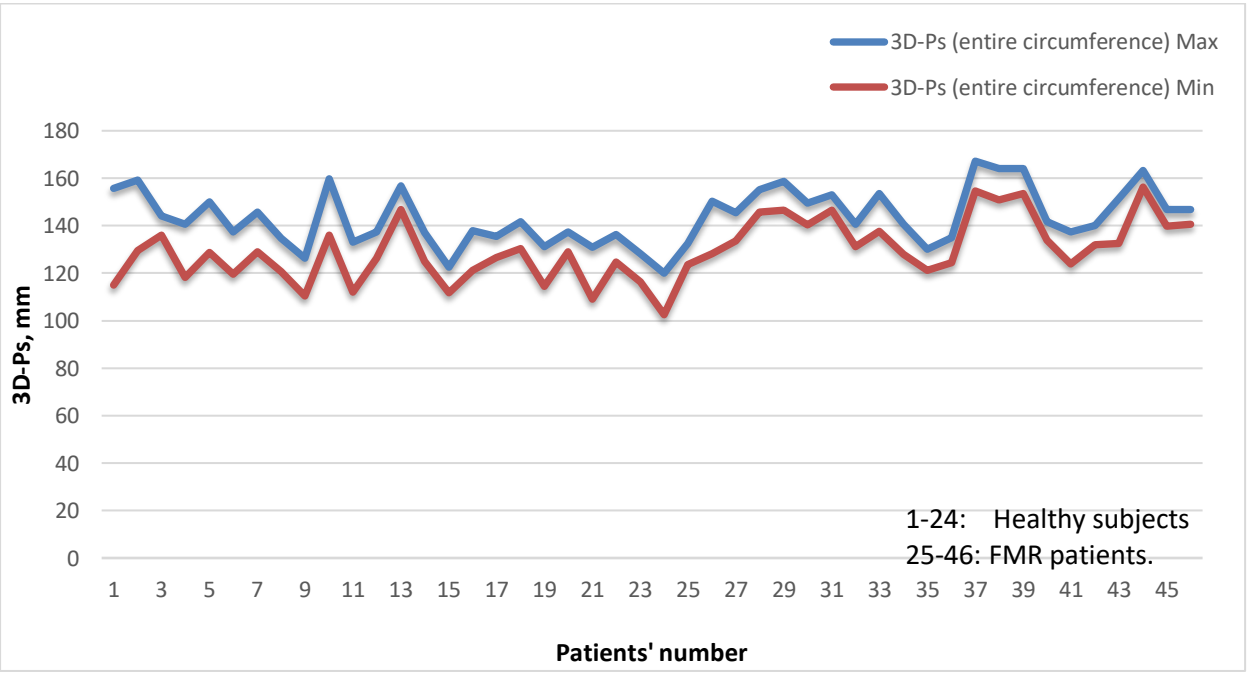

5. DISCUSSION

FMR is the second most common valvular heart disease whose prevalence is expected to grow due to the increasing life expectancies in the industrialized nations (5). Surgical or percutaneous interventions are available to treat severe symptomatic FMR (59, 83). To determine the best treatment for the patient and to improve clinical outcomes, the best approach for a comprehensive pre-procedural assessment of the MV and standardization of this approach must be defined. For instance, knowing the precise size of the MA is very important for successful MV replacements: using a larger-size valve reduces the risk for displacement toward the left atrium due to improved anchoring to the native mitral annulus; however, oversizing increases the risk of LVOT obstruction (84). Different imaging modalities and MA segmentation techniques have been reported. Due to the heterogeneity of the results of previous studies, the standardization of MV evaluation remains unclear.

5.1 Interpretation of the study results and their significance

Against the backdrop of the lacking consensus on how to measure the mitral valve in regards of planning for minimally invasive procedures, we comprehensively analyzed the mitral apparatus, its anatomy, geometry, mobility, as well as the spatial relationships between its components and surrounding structures, such as the atrioventricular conduction axis and the aortic valve.

The major findings of this study are:

(1) There are significant differences in the mitral annular morphology between healthy subjects and patients with FMR;
(2) When comparing the two mitral annulus models, the vast majority of parameters were higher for the saddle-shaped model compared to D-shaped model;
(3) 2D and 3D assessments of the mitral annular morphology throughout the cardiac cycle show differences between the MA circumferences;
(4) The more pronounced difference between the mean distance of the MA to the anterior papillary muscle vs. the mean distance of the MA to the posterior PM were observed in both groups;
(5) The mobility of the mitral annulus is higher in healthy subjects than in patients with FMR.

The results of the analysis presented here demonstrate that with good optimization of the procedural protocol and post-processing process, MSCT represents a feasible method for precisely evaluating the dimensions and mobility of the mitral valve.

In addition, in our study we included subjects with nearly the same mean BMI (≈26) as well as both genders in both groups to assess MV parameters more objectively for the general population. The number of male/female subjects in both groups was similar.

5.2. Comparison of results with earlier studies

No standardized method for assessing the mitral annulus has been defined. Although the saddle-shaped annulus is anatomically correct, some authors included the anterior horn of the MA (aortomitral continuity), while others did not. It should be noted that different devices may require specific measurements and D-shape annulus approach does not always correspond with the shape of device. Considering, different shape of devices and different parameters required for preprocedural assessment, the entire geometric shape of the MA needs to be considered when assessing for neo-LVOT obstruction. Blanke et al. hypothesized that MA must be modified by cutting off the aorto-mitral continuity and defining the anterior border of the MA as a virtual line connecting both trigones (planar D-shaped annulus) for pre-procedural device sizing in terms of avoiding LVOT obstruction (85). The proposal of Blanke et al. D-shaped model of MA was further used in a study by Abdelghani et al. (86). Measurements in both studies mentioned above were made only in diastolic phase of cardiac cycle. Good correlation was found for the annular dimension for D-shaped approach values. Unlike these studies, we reported saddle-shape annular dimensions including the aortomitral continuity and found considerable differences between the data obtained in our study and in the studies mentioned above due to different saddle-shaped annulus assessment approaches.

According to our data, the annulus area is considerably larger in the saddle-shaped MA model compared to the D-shaped model; this finding correlates closely with previous studies (44, 85, 87) in which aorto-mitral continuity was included. Based on our results and former clinical reports, we thus conclude that the saddle-shaped annulus area extends to the LVOT and may theoretically cause obstruction thereof.

No significant differences were ascertained regarding the average mean annular area, the 3D and 2D perimeters and the SL distance for both the saddle-shaped and D-shaped MA evaluation models in our study, compared to the results published by Blanke et al. (44). We have used the same technique and the same software (3mensio structural heart software (Pie Medical Imaging, Netherlands).

Study population in Alkadhi et al. study include control subjects, patients with cardiomyopathy (dilative and hypertrophic obstructive) and to assess the 3D MA area PointWrap Algorithm was

used (43). In comparison to our results, mean S-shaped MA area is without significant gap in control group and found to be bigger in patients with dilative cardiomyopathy.

They are significantly larger gap to MA area values between our study and results reported by Beaudoin et al. (88). In this study the annulus area was measured only in midsystole and total leaflet area was measured in diastole. Dedicated software (Omni4D, MD Handschumacher) was used.

In comparison to Alkadhi et al.(43) and Beaudoin et al.(88) differences in results are likely due to different assessment technique and different software used, since when using the same methodology and the same software, there is no marked difference in the results as in comparison to Blanke et al. study (44).

In agreement with a previous study of Mak et al., we found nearly similar results for the SL and TT distances and slightly different results for the annular area of the D-shaped mitral annulus mean for the FMR group in mid-diastole (87).

Delgado and colleagues reported that the area of the MA was significantly higher in heart failure patients compared to the control group, thus suggesting annular dilatation (7). The present study reported similar results.

Ormiston et al. reported changes in the annular area throughout the cardiac cycle as defined by echocardiography and measured maximum values for the annular area in late diastole and minimal values in mid systole already in 1981 (89). The largest mid-diastolic largest MA area was demonstrated later by other authors (43, 90, 91).

According to our study, the annular height of the saddle-shaped annulus was highest in diastole and lowest in mid-to-late systole. This finding proves flattening of the MA in the diastolic phase, as reported by Alkadhi et al. (43) and Blanke et al. (33). In FMR patients the saddle-shaped mitral annulus height decreases in general, resulting in a more planar annular contour according to a recent paper by Blanke et al. Furthermore, their investigation reported a mean MA area of the D-shaped annulus of 8.9 ±1.5 cm^2 in control subjects. The mean MA area was found to be slightly bigger in our study (10.3 ± 1.6 cm^2) (33).

Compared to our study, Theriault-Lauzier et al. provided MA data only for the diastolic phase, and only half of the cohort was additionally evaluated in systole (92). Important findings reported by the Theriault-Lauzier group, who compared the aorto-mitral angle between patients with and without FMR, included slight changes in systole and a decreased angle in the FMR group in diastole (92).

Our study clearly showed higher aorto-mitral annular angles in healthy subjects compared to patients with FMR; this picture was consistent through the cardiac cycle.

As part of the subvalvular assessment, the annulus-to-PM evaluation is important regarding the placement of the transcatheter device. It is referred to as an “obstacle-free zone” (73). We clearly showed a difference in the distance between the annulus and the anterior papillary muscle between the two groups, both in systole and in diastole, whereas the annulus-to-PM distance are nearly identical between the first and second group and differed only slightly between systole and diastole. Likewise, Theriault-Lauzier et al. showed a mild difference in the distance of the annulus to the anterior and posterior PM in systole and diastole; however, without distinguishing between the mean values of the groups with and without FMR, which was done in our study (92).

Considering all the findings detailed above, we assume good reproducibility of the assessment of most of the MV parameters in studies that are conducted with similar techniques.

The left atrium plays a key role in protecting the pulmonary vessels in mitral valve disease. Because the atrium becomes dysfunctional due to the regurgitant load, symptoms of pulmonary artery hypertension occur. An LA volume index > 60 ml/m² predicts an adverse cardiovascular outcome. In our study, the LA volume index in the FMR group was 81 ± 19.8 ml/m² vs. 41 ± 9.9 ml/m² in healthy subjects, which is in line with results reported by Ring L. and Le Tourneau T. (93, 94).

Furthermore, as an important part of the MV apparatus, in our study we also assessed LV hemodynamics and dimensions including LV long axis, LV sphericity index, and annulus to papillary muscles distances. As expected, we found pronounced higher than normal LV hemodynamics in the FMR group compared to the control group.

The LV sphericity index in systole and diastole are consistent with values published by the Di Donato and Delgado groups (7, 80) and was found to be higher in the FMR group owing to LV remodeling.

Several recent studies, such as Hulman et al. and Blanke et al., suggested using multiphase ECG-gated CT for a pre-procedural assessment of the mitral valve to choose the correct valve size (33, 84). Retrospective ECG-gated CTA is essential for obtaining both static and cine images. Cine clips obtained of each valve allow monitoring of valve motion. In our study, we also included a quantitative assessment of the valve mobility and compared the values measured in the control group and FMR group.

Our results showed that the mobility of the mitral annulus is much lower in FMR patients. Thus, multiphase ECG-gated preprocedural CT may not be necessary when planning transcatheter mitral valve procedures. Single- or dual-phase CT scans with prospective ECG synchronization can provide enough data for a pre-procedural analysis in such patients. Moreover, using such a

protocol can reduce the radiation exposure and risks. We assume that using multiphase CTA may still be beneficial in complicated cases, e.g. in patients with basal septal hypertrophy or prior aortic investigation or other unusual clinical scenarios, in order to prevent LVOT obstruction and to reduce risk of prosthetic valve mismatch.
Nonetheless, our data highlight the importance of a careful analysis with the potential to optimize pre-procedural exposure and reduce the dose of radiation and contrast media.

5.3 The advantages of CTA in evaluating the MV and comparison with other clinical imaging procedures

As stated in the previous section, it is necessary to take into account not only the mitral valvular apparatus when considering the relevant anatomy, but also the relationship between its components and the surrounding structures, such as the atrioventricular conduction axis, the aortic valve, the coronary sinus, and the circumflex coronary artery (5, 8). In comparison with echocardiography and CMR, CTA can provide such information with accurate 3D datasets of the cardiac morphology, excellent image quality, a higher spatial resolution and lower signal-to-noise ratio, a higher contrast between the cardiac chamber wall and blood flow (85, 87). Quantitative values relating to the LV function and muscle mass are independent predictors of cardiac morbidity and mortality. Hence, an accurate analysis of LV volumetric data is also very important and made possible by CTA. The data obtained by ECG-gated CTA is very comprehensive and may suffice for a pre-procedural analysis (88). At present, CT offers the highest 3D spatial resolution of all techniques (14). By performing MSCT for MV assessment, any findings which could exacerbate the MV procedure (e.g. pulmonary embolism, neoplastic processes, etc.) can be excluded in only one scan. Another advantage for patients with severe MR is that CTA provides all this data in a single breath hold (27, 34). It might also be useful to study dynamic changes in the regional LV function (6). Also, according to recent studies, this procedure has minimal operator dependence (73). Furthermore, CTA provides direct visualisation and quantification of mitral calcifications. Another advantages of pre-procedural cardiac CTA are the possibility to find an ideal access point to guide echocardiography by identifying the intended intraprocedural epicardial access point and to predict LVOT obstruction by preprocedural device simulation (95). Although CTA is associated with many advantages, we cannot ignore the fact that – compared to echocardiography and CMR – it involves radiation exposure and iodinated contrast injection in MSCT. However, an adjustment of protocols can keep the radiation dose within the permissible limits, resulting in a dose reduction of up to 50-70% and reducing the risk of contrast nephropathy (87). The main challenge in cardiac CT is

temporal resolution. Despite high spatial resolution, compared to echocardiography and CMR, CTA has lower temporal resolution (about 72 ms for modern dual-source scanners). However, using a dual-source scanner gives twice as good temporal resolution because data reconstruction is possible with only 90 tube rotation and the temporal resolution ≤ 80 ms is enough to get good quality images for assessing cardiac structures (45)

CT imaging is further influenced by artifacts caused by a rapid or irregular heart rhythm, which can affect the imaging quality of CT and represents another potential limitation/disadvantage.

Despite these disadvantages, when used appropriately, patients would most likely benefit from CT, especially elderly patients who are potential candidates for percutaneous minimally invasive procedures. Before such procedures all images should be carefully assessed for any incidental cardiac and extracardiac findings that may delay treatment or affect overall patient's prognosis and CTA can provide such assessment simultaneously.

5.4 Study limitations

The current study has some limitations. First, it was limited by its retrospective design. Second, only relatively few patients were included in each group. We included patients with FMR in the analysis, as these patients represent the group of patients that will potentially undergo TMVI in early clinical trials. Patients with degenerative MR or with extensive calcific changes of MA were not included in the analysis, representing another limitation. Despite the fact that all subjects in control group has no known cardiac abnormality or coronary artery disease, however, there is still remains a little uncertainty of cardiac health, some kind of myocardial diseases (myocarditis, cardiomyopathy etc.) in them are unlikely, but not completely excluded.In our study we did not evaluate the intercomissural distance of the MA or the distance from the MA to the circumflex artery and coronary sinus and the aorto-trigonal distance, which could be considered another weak point of our work. This is an important area that requires further research. Another limitation is that our study concentrated on establishing the pre-procedural post-processing technique without a correlation to the clinical outcome. The limited temporal resolution of CT can represent another limitation of our study.

However, to the extent of our knowledge, this is the first study that assesses and compares mitral valve dimensions and mobility, the subvalvular apparatus, LV hemodynamics, LA volume, aortomitral and LA-to-LV angles by MSCT in healthy subjects as controls and in patients with FMR, with most parameters evaluated through all phases of the cardiac cycle.

6. Conclusion

It is essential to optimise imaging acquisition protocols, in order to convey all relevant information for successful treatment planning. It should be noted that different devices may require specific measurements. Our data highlight the importance of a careful analysis with the potential to optimize pre-procedural exposure and reduce the dose of radiation and contrast media.The significant differences in the mitral annular morphology between healthy patients and patients with FMR were presented, along with several changes between different sizing approaches of the mitral annulus throughout the entire cardiac cycle.
A difference in the mobility of the mitral annulus was also identified; it is higher in healthy subjects than in patients with FMR. Considering the low mitral annulus mobility in patients with FMR and the relatively time-consuming assessment of mitral valve dimensions in all 10% phases of the RR interval using complex software, multiphase MSCT might not be necessary for planning transcatheter mitral valve interventions but may be replaced by dual-phase scans for example. This plays an important role in timing the pre-procedural analysis and determining the outcome of patients. Additionally, scans with lower number of phases would reduce radiation dose. However, using multiphase CTA should still be the favored mode in complicated cases.
In summary, our study demonstrates that a non-invasive, comprehensive assessment of the anatomy, geometry and dynamics of the mitral valve and of its relationships with the surrounding structures by MSCT is feasible. For translation of these results into the daily clinical routine, larger, comparative studies are warranted.

Bibliography (references)

1. Desai M, Jellis C, Yingchoncharoen T. An Atlas of Mitral Valve Imaging Springer, London; 2015. 281 p.
2. McCarthy KP, Ring L, Rana BS. Anatomy of the mitral valve: understanding the mitral valve complex in mitral regurgitation. Eur J Echocardiogr. 2010;11(10):i3-9.
3. Maisano F, Alfieri O, Banai S, Buchbinder M, Colombo A, Falk V, Feldman T, Franzen O, Herrmann H, Kar S, Kuck KH, Lutter G, Mack M, Nickenig G, Piazza N, Reisman M, Ruiz CE, Schofer J, Sondergaard L, Stone GW, Taramasso M, Thomas M, Vahanian A, Webb J, Windecker S, Leon MB. The future of transcatheter mitral valve interventions: competitive or complementary role of repair vs. replacement? Eur Heart J. 2015;36(26):1651-9.
4. Nkomo VT, Gardin JM, Skelton TN, Gottdiener JS, Scott CG, Enriquez-Sarano M. Burden of valvular heart diseases: a population-based study. Lancet. 2006;368(9540):1005-11.
5. Van Mieghem NM, Piazza N, Anderson RH, Tzikas A, Nieman K, De Laat LE, McGhie JS, Geleijnse ML, Feldman T, Serruys PW, de Jaegere PP. Anatomy of the mitral valvular complex and its implications for transcatheter interventions for mitral regurgitation. J Am Coll Cardiol. 2010;56(8):617-26.
6. Capoulade R, Piriou N, Serfaty JM, Le Tourneau T. Multimodality imaging assessment of mitral valve anatomy in planning for mitral valve repair in secondary mitral regurgitation. J Thorac Dis. 2017;9(Suppl 7):S640-S60.
7. Delgado V, Tops LF, Schuijf JD, de Roos A, Brugada J, Schalij MJ, Thomas JD, Bax JJ. Assessment of mitral valve anatomy and geometry with multislice computed tomography. JACC Cardiovasc Imaging. 2009;2(5):556-65.
8. Choure AJ, Garcia MJ, Hesse B, Sevensma M, Maly G, Greenberg NL, Borzi L, Ellis S, Tuzcu EM, Kapadia SR. In vivo analysis of the anatomical relationship of coronary sinus to mitral annulus and left circumflex coronary artery using cardiac multidetector computed tomography: implications for percutaneous coronary sinus mitral annuloplasty. J Am Coll Cardiol. 2006;48(10):1938-45.
9. Milind Desai CJ, Teerapat Yingchoncharoen. An atlas of mitral valve imaging: Springer London; 2016.
10. Dal-Bianco JP, Levine RA. Anatomy of the mitral valve apparatus: role of 2D and 3D echocardiography. Cardiol Clin. 2013;31(2):151-64.
11. Carpentier A. Cardiac valve surgery--the "French correction". J Thorac Cardiovasc Surg. 1983;86(3):323-37.

12. Carpentier AF, Lessana A, Relland JY, Belli E, Mihaileanu S, Berrebi AJ, Palsky E, Loulmet DF. The "physio-ring": an advanced concept in mitral valve annuloplasty. Ann Thorac Surg. 1995;60(5):1177-85; discussion 85-6.
13. Dal-Bianco JP, Aikawa E, Bischoff J, Guerrero JL, Handschumacher MD, Sullivan S, Johnson B, Titus JS, Iwamoto Y, Wylie-Sears J, Levine RA, Carpentier A. Active adaptation of the tethered mitral valve: insights into a compensatory mechanism for functional mitral regurgitation. Circulation. 2009;120(4):334-42.
14. Li CH, Arzamendi D, Carreras F. Role of Imaging Techniques in Percutaneous Treatment of Mitral Regurgitation. Rev Esp Cardiol (Engl Ed). 2016;69(4):421-36.
15. Berdajs D, Lajos P, Turina MI. A new classification of the mitral papillary muscle. Med Sci Monit. 2005;11(1):BR18-21.
16. Victor S, Nayak VM. Variations in the papillary muscles of the normal mitral valve and their surgical relevance. J Card Surg. 1995;10(5):597-607.
17. Natarajan N, Patel P, Bartel T, Kapadia S, Navia J, Stewart W, Tuzcu EM, Schoenhagen P. Peri-procedural imaging for transcatheter mitral valve replacement. Cardiovasc Diagn Ther. 2016;6(2):144-59.
18. Lam JH, Ranganathan N, Wigle ED, Silver MD. Morphology of the human mitral valve. I. Chordae tendineae: a new classification. Circulation. 1970;41(3):449-58.
19. Silbiger JJ, Bazaz R. Contemporary insights into the functional anatomy of the mitral valve. Am Heart J. 2009;158(6):887-95.
20. Dal-Bianco JP, Beaudoin J, Handschumacher MD, Levine RA. Basic mechanisms of mitral regurgitation. Can J Cardiol. 2014;30(9):971-81.
21. Enriquez-Sarano M, Akins CW, Vahanian A. Mitral regurgitation. Lancet. 2009;373(9672):1382-94.
22. Levine RA, Hagege AA, Judge DP, Padala M, Dal-Bianco JP, Aikawa E, Beaudoin J, Bischoff J, Bouatia-Naji N, Bruneval P, Butcher JT, Carpentier A, Chaput M, Chester AH, Clusel C, Delling FN, Dietz HC, Dina C, Durst R, Fernandez-Friera L, Handschumacher MD, Jensen MO, Jeunemaitre XP, Le Marec H, Le Tourneau T, Markwald RR, Merot J, Messas E, Milan DP, Neri T, Norris RA, Peal D, Perrocheau M, Probst V, Puceat M, Rosenthal N, Solis J, Schott JJ, Schwammenthal E, Slaugenhaupt SA, Song JK, Yacoub MH, Leducq Mitral Transatlantic N. Mitral valve disease--morphology and mechanisms. Nat Rev Cardiol. 2015;12(12):689-710.
23. Ted Feldman OF, Reginald Low, Jason Rogers, Khung Keong Yeo. Atlas of percutaneous mitral valve repair.: Springer London; 2013.

24. Adams DH, Rosenhek R, Falk V. Degenerative mitral valve regurgitation: best practice revolution. Eur Heart J. 2010;31(16):1958-66.
25. Levine RA, Triulzi MO, Harrigan P, Weyman AE. The relationship of mitral annular shape to the diagnosis of mitral valve prolapse. Circulation. 1987;75(4):756-67.
26. Hjortnaes J, Keegan J, Bruneval P, Schwartz E, Schoen FJ, Carpentier A, Levine RA, Hagege A, Aikawa E. Comparative Histopathological Analysis of Mitral Valves in Barlow Disease and Fibroelastic Deficiency. Semin Thorac Cardiovasc Surg. 2016;28(4):757-67.
27. Borger MA, Alam A, Murphy PM, Doenst T, David TE. Chronic ischemic mitral regurgitation: repair, replace or rethink? Ann Thorac Surg. 2006;81(3):1153-61.
28. Debonnaire P, Al Amri I, Leong DP, Joyce E, Katsanos S, Kamperidis V, Schalij MJ, Bax JJ, Marsan NA, Delgado V. Leaflet remodelling in functional mitral valve regurgitation: characteristics, determinants, and relation to regurgitation severity. Eur Heart J Cardiovasc Imaging. 2015;16(3):290-9.
29. Grande-Allen KJ, Borowski AG, Troughton RW, Houghtaling PL, Dipaola NR, Moravec CS, Vesely I, Griffin BP. Apparently normal mitral valves in patients with heart failure demonstrate biochemical and structural derangements: an extracellular matrix and echocardiographic study. J Am Coll Cardiol. 2005;45(1):54-61.
30. Levine RA, Schwammenthal E. Ischemic mitral regurgitation on the threshold of a solution: from paradoxes to unifying concepts. Circulation. 2005;112(5):745-58.
31. Delgado V, Kapadia S, Marsan NA, Schalij MJ, Tuzcu EM, Bax JJ. Multimodality imaging before, during, and after percutaneous mitral valve repair. Heart. 2011;97(20):1704-14.
32. Manghat NE, Rachapalli V, Van Lingen R, Veitch AM, Roobottom CA, Morgan-Hughes GJ. Imaging the heart valves using ECG-gated 64-detector row cardiac CT. Br J Radiol. 2008;81(964):275-90.
33. Blanke P, Naoum C, Webb J, Dvir D, Hahn RT, Grayburn P, Moss RR, Reisman M, Piazza N, Leipsic J. Multimodality Imaging in the Context of Transcatheter Mitral Valve Replacement: Establishing Consensus Among Modalities and Disciplines. JACC Cardiovasc Imaging. 2015;8(10):1191-208.
34. Guo YK, Yang ZG, Ning G, Rao L, Dong L, Pen Y, Zhang TM, Wu Y, Zhang XC, Wang QL. Sixty-four-slice multidetector computed tomography for preoperative evaluation of left ventricular function and mass in patients with mitral regurgitation: comparison with magnetic resonance imaging and echocardiography. Eur Radiol. 2009;19(9):2107-16.
35. Chen JJ, Manning MA, Frazier AA, Jeudy J, White CS. CT angiography of the cardiac valves: normal, diseased, and postoperative appearances. Radiographics. 2009;29(5):1393-412.

36. Child N, Suna G, Dabir D, Yap ML, Rogers T, Kathirgamanathan M, Arroyo-Ucar E, Hinojar R, Mahmoud I, Young C, Wendler O, Mayr M, Sandhu B, Morton G, Muhly-Reinholz M, Dimmeler S, Nagel E, Puntmann VO. Comparison of MOLLI, shMOLLLI, and SASHA in discrimination between health and disease and relationship with histologically derived collagen volume fraction. Eur Heart J Cardiovasc Imaging. 2018;19(7):768-76.
37. François CJ. Current state of the art cardiovascular MR imaging techniques for assessment of ischemic heart disease. Radiol Clin North Am. 2015;53(2):335-44.
38. h-Ici DO, Jeuthe S, Al-Wakeel N, Berger F, Kuehne T, Kozerke S, Messroghli DR. T1 mapping in ischaemic heart disease. Eur Heart J Cardiovasc Imaging. 2014;15(6):597-602.
39. De Araujo Goncalves P, Campos CAM, Serruys PW, Garcia-Garcia HM. Computed tomography angiography for the interventional cardiologist. European Heart Journal - Cardiovascular Imaging. 2014;15(8):842-54.
40. Lin E, Alessio A. What are the basic concepts of temporal, contrast, and spatial resolution in cardiac CT? Journal of Cardiovascular Computed Tomography. 2009;3(6):403-8.
41. Van Mieghem NM, Rodriguez-Olivares R, Ren BC, van Gils L, Maugenest A, Geleijnse ML, Budde RP, Vogelaar J, Verstraeten L, de Jaegere PP. Computed tomography optimised fluoroscopy guidance for transcatheter mitral therapies. EuroIntervention. 2016;11(12):1428-31.
42. Faggioni L, Gabelloni M, Accogli S, Angelillis M, Costa G, Spontoni P, Petronio AS, Caramella D. Preprocedural planning of transcatheter mitral valve interventions by multidetector CT: What the radiologist needs to know. European Journal of Radiology Open. 2018;5:131-40.
43. Alkadhi H, Desbiolles L, Stolzmann P, Leschka S, Scheffel H, Plass A, Schertler T, Trindade PT, Genoni M, Cattin P, Marincek B, Frauenfelder T. Mitral annular shape, size, and motion in normals and in patients with cardiomyopathy: evaluation with computed tomography. Invest Radiol. 2009;44(4):218-25.
44. Blanke P, Dvir D, Cheung A, Ye J, Levine RA, Precious B, Berger A, Stub D, Hague C, Murphy D, Thompson C, Munt B, Moss R, Boone R, Wood D, Pache G, Webb J, Leipsic J. A simplified D-shaped model of the mitral annulus to facilitate CT-based sizing before transcatheter mitral valve implantation. J Cardiovasc Comput Tomogr. 2014;8(6):459-67.
45. Commandeur F, Goeller M, Dey D. Cardiac CT: Technological Advances in Hardware, Software, and Machine Learning Applications. Curr Cardiovasc Imaging Rep. 2018;11.
46. Agricola E, Oppizzi M, Pisani M, Meris A, Maisano F, Margonato A. Ischemic mitral regurgitation: mechanisms and echocardiographic classification. Eur J Echocardiogr. 2008;9(2):207-21.

47. Asgar AW, Mack MJ, Stone GW. Secondary mitral regurgitation in heart failure: pathophysiology, prognosis, and therapeutic considerations. J Am Coll Cardiol. 2015;65(12):1231-48.
48. Jaffe LM, Morin DP. Cardiac resynchronization therapy: history, present status, and future directions. Ochsner J. 2014;14(4):596-607.
49. Ogutu P, Ahmed I, Dunning J. Should patients with asymptomatic severe mitral regurgitation with good left ventricular function undergo surgical repair? Interact Cardiovasc Thorac Surg. 2010;10(2):299-305.
50. Beaudoin J, Singh JP, Szymonifka J, Zhou Q, Levine RA, Januzzi JL, Truong QA. Novel Heart Failure Biomarkers Predict Improvement of Mitral Regurgitation in Patients Receiving Cardiac Resynchronization Therapy-The BIOCRT Study. Can J Cardiol. 2016;32(12):1478-84.
51. Mihos CG, Yucel E, Capoulade R, Orencole MP, Upadhyay GA, Santana O, Singh JP, Picard MH. Impact of cardiac resynchronization therapy on mitral valve apparatus geometry and clinical outcomes in patients with secondary mitral regurgitation. Echocardiography. 2017.
52. Taramasso M, Buzzatti N, La Canna G, Colombo A, Alfieri O, Maisano F. Interventional vs. surgical mitral valve therapy. Which technique for which patient? Herz. 2013;38(5):460-6.
53. Kang DH, Heo R, Lee S, Baek S, Kim DH, Song JM, Song JK, Lee JW. Initial surgery versus conservative management of symptomatic severe mitral regurgitation in the elderly. Heart. 2018;104(10):849-54.
54. Detter C, Boehm DH, Reichenspurner H. Minimally invasive valve surgery: different techniques and approaches. Expert Rev Cardiovasc Ther. 2004;2(2):239-51.
55. Woo YJ. Minimally invasive valve surgery. Surg Clin North Am. 2009;89(4):923-49, x.
56. Seeburger J, Falk V, Borger MA, Passage J, Walther T, Doll N, Mohr FW. Chordae replacement versus resection for repair of isolated posterior mitral leaflet prolapse: à ègalité. Ann Thorac Surg. 2009;87(6):1715-20.
57. Wu AH, Aaronson KD, Bolling SF, Pagani FD, Welch K, Koelling TM. Impact of mitral valve annuloplasty on mortality risk in patients with mitral regurgitation and left ventricular systolic dysfunction. J Am Coll Cardiol. 2005;45(3):381-7.
58. Bax JJ, Braun J, Somer ST, Klautz R, Holman ER, Versteegh MI, Boersma E, Schalij MJ, van der Wall EE, Dion RA. Restrictive annuloplasty and coronary revascularization in ischemic mitral regurgitation results in reverse left ventricular remodeling. Circulation. 2004;110(11 Suppl 1):II103-8.
59. Acker MA, Parides MK, Perrault LP, Moskowitz AJ, Gelijns AC, Voisine P, Smith PK, Hung JW, Blackstone EH, Puskas JD, Argenziano M, Gammie JS, Mack M, Ascheim DD,

Bagiella E, Moquete EG, Ferguson TB, Horvath KA, Geller NL, Miller MA, Woo YJ, D'Alessandro DA, Ailawadi G, Dagenais F, Gardner TJ, O'Gara PT, Michler RE, Kron IL, Ctsn. Mitral-valve repair versus replacement for severe ischemic mitral regurgitation. N Engl J Med. 2014;370(1):23-32.
60. Maisano F, Vigano G, Calabrese C, Taramasso M, Denti P, Blasio A, Guidotti A, Alfieri O. Quality of life of elderly patients following valve surgery for chronic organic mitral regurgitation. Eur J Cardiothorac Surg. 2009;36(2):261-6; discussion 6.
61. Detaint D, Sundt TM, Nkomo VT, Scott CG, Tajik AJ, Schaff HV, Enriquez-Sarano M. Surgical correction of mitral regurgitation in the elderly: outcomes and recent improvements. Circulation. 2006;114(4):265-72.
62. McGee EC, Gillinov AM, Blackstone EH, Rajeswaran J, Cohen G, Najam F, Shiota T, Sabik JF, Lytle BW, McCarthy PM, Cosgrove DM. Recurrent mitral regurgitation after annuloplasty for functional ischemic mitral regurgitation. J Thorac Cardiovasc Surg. 2004;128(6):916-24.
63. Nissinen J, Biancari F, Wistbacka JO, Peltola T, Loponen P, Tarkiainen P, Virkkilä M, Tarkka M. Safe time limits of aortic cross-clamping and cardiopulmonary bypass in adult cardiac surgery. Perfusion. 2009;24(5):297-305.
64. Anwer LA, Dearani JA, Daly RC, Stulak JM, Schaff HV, Nguyen A, Toeg H, Topilsky Y, Michelena HI, Eleid MF, Maltais S. Degenerative Mitral Regurgitation After Non-Mitral Cardiac Surgery: MitraClip Versus Surgical Reconstruction. Ann Thorac Surg. 2018.
65. Maisano F, Godino C, Giacomini A, Denti P, Arendar I, Buzzatti N, Canna GL, Alfieri O, Colombo A. Clinical trial experience with the MitraClip catheter based mitral valve repair system. Int J Cardiovasc Imaging. 2011;27(8):1155-64.
66. Pighi M, Estevez-Loureiro R, Maisano F, Ussia GP, Dall'Ara G, Franzen O, Laroche C, Settergren M, Winter R, Nickenig G, Gilard M, Di Mario C, Transcatheter Valve Treatment Sentinel Registry Investigators of the ERPotESoC. Immediate and 12-Month Outcomes of Ischemic Versus Nonischemic Functional Mitral Regurgitation in Patients Treated With MitraClip (from the 2011 to 2012 Pilot Sentinel Registry of Percutaneous Edge-To-Edge Mitral Valve Repair of the European Society of Cardiology). Am J Cardiol. 2017;119(4):630-7.
67. Inderbitzin DT, Taramasso M, Nietlispach F, Maisano F. Percutaneous Mitral Valve Repair with MitraClip: Patient and Valve Selection for Optimal Outcome. Curr Cardiol Rep. 2016;18(12):129.

68. Maisano F, Denti P, Michev I, La Canna G, Arendar I, Colombo A, Alfieri O. Percutaneous mitral valve repair with the edge-to-edge technique. Multimed Man Cardiothorac Surg. 2010;2010(316):mmcts 2009 004002.
69. Van Praet KM, Stamm C, Sündermann SH, Meyer A, Unbehaun A, Montagner M, Nazari Shafti TZ, Jacobs S, Falk V, Kempfert J. Minimally Invasive Surgical Mitral Valve Repair: State of the Art Review. Interv Cardiol. 2018;13(1):14-9.
70. Mylotte D, Piazza N. Transcatheter mitral valve implantation: a brief review. EuroIntervention. 2015;11 Suppl W:W67-70.
71. Piazza N, Asgar A, Ibrahim R, Bonan R. Transcatheter mitral and pulmonary valve therapy. J Am Coll Cardiol. 2009;53(20):1837-51.
72. Nishimura RA, Otto CM, Bonow RO, Carabello BA, Erwin JP, Fleisher LA, Jneid H, Mack MJ, McLeod CJ, O'Gara PT, Rigolin VH, Sundt TM, Thompson A. 2017 AHA/ACC Focused Update of the 2014 AHA/ACC Guideline for the Management of Patients With Valvular Heart Disease: A Report of the American College of Cardiology/American Heart Association Task Force on Clinical Practice Guidelines. J Am Coll Cardiol. 2017;70(2):252-89.
73. Theriault-Lauzier P, Mylotte D, Dorfmeister M, Spaziano M, Andalib A, Mamane S, Chetrit M, Blanke P, Cecere R, Buithieu J, Martucci G, Tchetche D, Modine T, van Mieghem N, Lange R, Windecker S, Bilodeau L, Leipsic J, Piazza N. Quantitative multi-slice computed tomography assessment of the mitral valvular complex for transcatheter mitral valve interventions part 1: systematic measurement methodology and inter-observer variability. EuroIntervention. 2016;12(8):e1011-e20.
74. Abdelghani M, Onuma Y, Zeng Y, Soliman OI, Ma J, Huo Y, Guidotti A, Nietlispach F, Maisano F, Serruys PW. The Sino Medical AccuFit transcatheter mitral valve implantation system. EuroIntervention. 2015;11 Suppl W:W84-5.
75. Piazza N, Treede H, Moat N, Sorajja P, Popma J, Grube E, Bolling S, Adams D. The Medtronic transcatheter mitral valve implantation system. EuroIntervention. 2015;11 Suppl W:W80-1.
76. Bapat V, Lim ZY, Boix R, Pirone F. The Edwards Fortis transcatheter mitral valve implantation system. EuroIntervention. 2015;11 Suppl W:W73-5.
77. Perpetua EM, Reisman M. The Tendyne transcatheter mitral valve implantation system. EuroIntervention. 2015;11 Suppl W:W78-9.
78. Sondergaard L, Ussia GP, Dumonteil N, Quadri A. The CardiAQ transcatheter mitral valve implantation system. EuroIntervention. 2015;14(W):W76-W7.

79. Verheye S, Cheung A, Leon M, Banai S. The Tiara transcatheter mitral valve implantation system. EuroIntervention. 2015;11 Suppl W:W71-2.
80. Di Donato M, Dabic P, Castelvecchio S, Santambrogio C, Brankovic J, Collarini L, Joussef T, Frigiola A, Buckberg G, Menicanti L. Left ventricular geometry in normal and post-anterior myocardial infarction patients: sphericity index and 'new' conicity index comparisons. Eur J Cardiothorac Surg. 2006;29 Suppl 1:S225-30.
81. Lester SJ, Ryan EW, Schiller NB, Foster E. Best method in clinical practice and in research studies to determine left atrial size. Am J Cardiol. 1999;84(7):829-32.
82. de Vaan J, Verstraeten L, de Jaegere P, Schultz C. The 3mensio Valves multimodality workstation. EuroIntervention. 2012;7(12):1464-9.
83. Asgar AW, Khairy P. Percutaneous repair or surgery for mitral regurgitation. N Engl J Med. 2011;365(1):90; author reply 1.
84. Hulman M, Bena M, Artemiou P, Gasparovic I, Hudec V, Rajani R, Bapat V. Iterative Learning of Transcatheter Mitral Valve Replacement in Mitral Valve Annulus Calcification: Management and Prevention of Transcatheter Mitral Valve Replacement Dislocation. Ann Thorac Surg. 2016;102(4):e287-90.
85. Blanke P, Dvir D, Cheung A, Levine RA, Thompson C, Webb JG, Leipsic J. Mitral Annular Evaluation With CT in the Context of Transcatheter Mitral Valve Replacement. JACC Cardiovasc Imaging. 2015;8(5):612-5.
86. Abdelghani M, Spitzer E, Soliman OII, Beitzke D, Laggner R, Cavalcante R, Tateishi H, Campos CM, Verstraeten L, Sotomi Y, Tenekecioglu E, Onuma Y, Tijssen JG, de Winter RJ, Maisano F, Serruys PW. A simplified and reproducible method to size the mitral annulus: implications for transcatheter mitral valve replacement. Eur Heart J Cardiovasc Imaging. 2017;18(6):697-706.
87. Mak GJ, Blanke P, Ong K, Naoum C, Thompson CR, Webb JG, Moss R, Boone R, Ye J, Cheung A, Munt B, Leipsic J, Grewal J. Three-Dimensional Echocardiography Compared With Computed Tomography to Determine Mitral Annulus Size Before Transcatheter Mitral Valve Implantation. Circ Cardiovasc Imaging. 2016;9(6).
88. Beaudoin J, Thai WE, Wai B, Handschumacher MD, Levine RA, Truong QA. Assessment of mitral valve adaptation with gated cardiac computed tomography: validation with three-dimensional echocardiography and mechanistic insight to functional mitral regurgitation. Circ Cardiovasc Imaging. 2013;6(5):784-9.

89. Ormiston JA, Shah PM, Tei C, Wong M. Size and motion of the mitral valve annulus in man. I. A two-dimensional echocardiographic method and findings in normal subjects. Circulation. 1981;64(1):113-20.
90. Flachskampf FA, Chandra S, Gaddipatti A, Levine RA, Weyman AE, Ameling W, Hanrath P, Thomas JD. Analysis of shape and motion of the mitral annulus in subjects with and without cardiomyopathy by echocardiographic 3-dimensional reconstruction. J Am Soc Echocardiogr. 2000;13(4):277-87.
91. Mihaila S, Muraru D, Miglioranza MH, Piasentini E, Peluso D, Cucchini U, Iliceto S, Vinereanu D, Badano LP. Normal mitral annulus dynamics and its relationships with left ventricular and left atrial function. Int J Cardiovasc Imaging. 2015;31(2):279-90.
92. Theriault-Lauzier P, Dorfmeister M, Mylotte D, Andalib A, Spaziano M, Blanke P, Martucci G, Lange R, Leipsic J, Bilodeau L, Piazza N. Quantitative multi-slice computed tomography assessment of the mitral valvular complex for transcatheter mitral valve interventions part 2: geometrical measurements in patients with functional mitral regurgitation. EuroIntervention. 2016;12(8):e1021-e30.
93. Ring L, Rana BS, Wells FC, Kydd AC, Dutka DP. Atrial function as a guide to timing of intervention in mitral valve prolapse with mitral regurgitation. JACC Cardiovasc Imaging. 2014;7(3):225-32.
94. Le Tourneau T, Messika-Zeitoun D, Russo A, Detaint D, Topilsky Y, Mahoney DW, Suri R, Enriquez-Sarano M. Impact of left atrial volume on clinical outcome in organic mitral regurgitation. J Am Coll Cardiol. 2010;56(7):570-8.
95. Blanke P, Park JK, Grayburn P, Naoum C, Ong K, Kohli K, Norgaard BL, Webb JG, Popma J, Boshell D, Sorajja P, Muller D, Leipsic J. Left ventricular access point determination for a coaxial approach to the mitral annular landing zone in transcatheter mitral valve replacement. J Cardiovasc Comput Tomogr. 2017;11(4):281-7.

Affidavit

Eidesstattliche Versicherung

„Ich, Leyla Musayeva, versichere an Eides statt durch meine eigenhändige Unterschrift, dass ich die vorgelegte Dissertation mit dem Thema:

“Quantitative evaluation of the mitral valve anatomy, geometry and spatial relationships in multiple cardiac phases by multi-slice computed tomography for planning of minimal invasive or percutaneous interventions.”

selbstständig und ohne nicht offengelegte Hilfe Dritter verfasst und keine anderen als die angegebenen Quellen und Hilfsmittel genutzt habe.
Alle Stellen, die wörtlich oder dem Sinne nach auf Publikationen oder Vorträgen anderer Autoren beruhen, sind als solche in korrekter Zitierung kenntlich gemacht. Die Abschnitte zu Methodik (insbesondere praktische Arbeiten, Laborbestimmungen, statistische Aufarbeitung) und Resultaten (insbesondere Abbildungen, Graphiken und Tabellen werden von mir verantwortet.
Meine Anteile an etwaigen Publikationen zu dieser Dissertation entsprechen denen, die in der untenstehenden gemeinsamen Erklärung mit dem/der Betreuer/in, angegeben sind. Für sämtliche im Rahmen der Dissertation entstandenen Publikationen wurden die Richtlinien des ICMJE (International Committee of Medical Journal Editors; www.icmje.og) zur Autorenschaft eingehalten. Ich erkläre ferner, dass mir die Satzung der Charité – Universitätsmedizin Berlin zur Sicherung Guter Wissenschaftlicher Praxis bekannt ist und ich mich zur Einhaltung dieser Satzung verpflichte.
Die Bedeutung dieser eidesstattlichen Versicherung und die strafrechtlichen Folgen einer unwahren eidesstattlichen Versicherung (§156,161 des Strafgesetzbuches) sind mir bekannt und bewusst.“

Datum Unterschrift

Curriculum Vitae

My curriculum vitae does not appear in the electronic version of my paper for reasons of data protection.

Acknowledgements

Firstly, I would like to express my sincere gratitude to my supervisor Priv.-Doz. Dr. med. Simon Sündermann for sharing his experience and helping me with every question or trouble I had through my research or writing the thesis. He consistently allowed this paper to be my own work, but steered me in right direction, whenever needed. This accomplishment would have not been possible without his outstanding contribution.

My sincere thanks also go to my supervisors Prof. Dr. med. Volkmar Falk and Prof. Dr. med. Jörg Kempfert for their continuous support and warm encouragement. Their guidance helped me in all the time of research.

I am gratefully indebted to Dr. Natalja Solowjowa for providing me with all necessary facilities in DHZB for making this research.

I am very thankful to Ms. Sarah Chalmers for revision of my thesis and for her very valuable comments on English correction of this thesis.

I would also like to thank Ms. Astrid Benhennour who helped me by giving instructions for making literature citations in accordance with international regulations.

Finally, I take this opportunity to express gratitude to my family and friends for their help, unceasing encouragement and support.